

ABSTRACT

MORALES, JUSTIN RICHARD. Manufacturing Boron Nitride Nanotube (BNNT) Reinforced Polymer Derived Ceramic (PDC) Composites for Space Applications. (Under the direction of Dr. Cheryl Xu).

Future deep space missions, such as the mission to Mars, will be very dangerous due to space hazards such as micro-meteorites and ionizing radiation. These missions will require advanced materials to survive the harsh environment of space. This work aims to develop a multifunctional ceramic composite that can be integrated into current space technologies including entry, descent, and landing (EDL) systems, astronaut suits, and inflatable space structures. The ultimate goal is to develop a composite with the following properties: excellent toughness, high thermal stability, and efficient space radiation shielding.

Boron nitride nanotubes (BNNTs) are a new type of nanomaterial with incredible properties. Such properties include high thermal stability (up to 900 °C in air), high elastic modulus (~1 TPa), and the ability to shield neutron radiation. These properties make BNNTs an ideal reinforcing material for space application. Polymer derived ceramics (PDCs) are a unique type of ceramic that are produced by the thermal decomposition of polymer precursors. They are known for their advanced thermal-mechanical properties such as their excellent oxidation and creep resistance at ultrahigh temperatures (up to 2000 °C). Creating a BNNT-PDC material would combine all these incredible properties to create an advanced composite suitable for space.

In this thesis, four different manufacturing methods were investigated to create BNNT-PDC composites. The objective of this research is to discover an optimal composite manufacturing method with effective BNNT dispersion and improved mechanical properties. The first method involves mixing the BNNTs with preceramic powder via ball-milling. These composites showed a 200% increase in hardness, but the BNNT dispersion was poor, and the nanotubes were potentially damaged from excessive ball-milling. The second method uses polymer infiltration to

reinforce BNNT mats. These composites had high BNNT weight percentages (up to 35 wt%) but there was no improvement in mechanical properties when compared to the pristine ceramic. The third method mixes the BNNT directly in the liquid precursor. These composites had very low BNNT weight percentages (up to 0.5 wt%) and only increased hardness by 5.8%. The final method uses ethanol to mix the BNNTs and preceramic powder together. This method showed excellent BNNT dispersion in the ceramic powder and preliminary mechanical tests suggest the composite's hardness increased over 400% compared to the pristine ceramic. The final method showed promising results and should be used to manufacture future BNNT ceramic composites.

© Copyright 2021 by Justin Richard Morales

All Rights Reserved

Manufacturing Boron Nitride Nanotube (BNNT) Reinforced Polymer Derived Ceramic
(PDC) Composites for Space Applications

by
Justin Richard Morales

A thesis submitted to the Graduate Faculty of
North Carolina State University
in partial fulfillment of the
requirements for the degree of
Master of Science

Mechanical Engineering

Raleigh, North Carolina
2021

APPROVED BY:

Dr. Cheryl Xu
Committee Chair

Dr. Fuh-Gwo Yuan

Dr. Andre Mazzoleni

Dr. Cheol Park
External Member

Dr. Sang-Hyon Chu
External Member

DEDICATION

To my parents and my sister

&

To the next giant leap for mankind

BIOGRAPHY

Justin Richard Morales was born and raised in Miami, Florida. In 2017, he earned his bachelor's degree in Mechanical Engineering at Florida State University. While at Florida State University, he joined Dr. Cheryl's Xu's lab group as an undergraduate researcher where he was first exposed to polymer derived ceramics and began his journey manufacturing advanced ceramic composites. During the summer of 2017, he was given an internship opportunity to go to NASA Langley Research Center (Virginia) to test a few ceramic composites made in Dr. Xu's lab. In 2018, Dr. Xu's research group moved to North Carolina State University. He followed her group and began his master's degree in Mechanical Engineering in the fall of 2018. He completed his first year of graduate studies and then took a year off from school to intern at NASA Langley again. While at NASA Langley, he was able to continue his research on manufacturing ceramic composites reinforced with nanotubes.

ACKNOWLEDGMENTS

Firstly, I would like to thank my thesis advisor, Dr. Cheryl Xu, for inspiring me to pursue my master's degree and giving me the opportunity to research in the Artificial Intelligence – Assisted Multifunctional Materials Manufacturing (AI-M3) Lab. Her guidance and support helped me tremendously during my research and graduate studies. I am also thankful for her giving me the platform to enhance my research and career skills.

I am also thankful for my mentors at NASA Langley, Dr. Cheol Park and Dr. Sang-Hyon Chu. They have followed and inspired me since the beginning of my research journey. Their guidance and insight helped me become a better researcher. This research would have not been possible without their support. I am extremely grateful for everything they have done for me and my career. I would also like to thank Dr. Fuh-Gwo Yuan and Dr. Andre Mazzoleni for being a part of my thesis committee. I am grateful for their time and effort in reviewing my thesis.

I am very grateful to the Mechanical and Aerospace Engineering department for giving me the opportunity to pursue my master's degree at North Carolina State University. I am thankful for all the NCSU, AIF, and NASA members that helped me with sample characterization and testing. I would like to thank my fellow lab mates, Atiqur Chowdhury and Tosin Ajayi, for their friendship and support for the past few years.

Last but not least, I would like to thank my parents. They have sacrificed so much for me and raised me to be the man I am today. Without their constant support, this would have not been possible. I would also like to thank my little sister along with all my family and friends that supported me through this journey.

This research was funded by NCSU's Graduate Student Support Plan (GSSP), NASA Internships Fellowships & Scholarships (NIFS) program, NC Space Grant Graduate Research Fellowship program, and Christopher Newport University Internship program.

TABLE OF CONTENTS

LIST OF TABLES	viii
LIST OF FIGURES	ix
Chapter 1: Introduction	1
1.1 Space Environment	1
1.2 Proposed Material	3
1.3 Research Objectives	3
1.4 Thesis Outline	4
Chapter 2: Literature Review	6
2.1 Introduction to Polymer Derived Ceramics (PDCs)	6
2.1.1 Polymer Precursor	7
2.1.2 Curing: Polymer Shaping and Cross-linking	9
2.1.3 Pyrolysis: Polymer to Ceramic Transformation	11
2.1.4 Fillers	13
2.1.5 Mechanical Properties of PDCs	15
2.2 Introduction to Boron Nitride Nanotubes (BNNTs)	17
2.2.1 BNNT Manufacturing and Quality	19
2.2.2 BNNT Paper (mat)	20
2.2.3 BNNT Neutron Shielding Ability	21
2.3 Introduction to Composites	23
2.3.1 Ceramic Matrix Composites (CMCs)	24
2.3.2 BNNT Reinforced Composites	26
Chapter 3: Ball-milling Mixing Method	28
3.1 Introduction	28
3.2 Experimental	29
3.3 Results	30
3.4 Summary	35
Chapter 4: Polymer Infiltration and Pyrolysis (PIP) Method	37
4.1 Introduction	37
4.2 Experimental	39
4.3 Results	42

4.4 Summary	45
Chapter 5: Precursor Mixing Method	47
5.1 Introduction.....	47
5.2 Experimental	47
5.3 Results.....	49
5.4 Summary	53
Chapter 6: Ethanol Mixing Method	54
6.1 Introduction.....	54
6.2 Experimental	54
6.3 Results.....	57
6.4 Summary	63
Chapter 7: Conclusion	64
7.1 Review of Manufacturing Methods	64
7.2 Future Work	67
References	69

LIST OF TABLES

Table 1. Mechanical properties of bulk Si-C-N systems	16
Table 2. CNT and BNNT properties.....	18
Table 3. Sintering conditions and mechanical properties of BNNT ceramic composites	27
Table 4. Ball-milling mixing sample measurements	32
Table 5. Vickers Hardness Results for ball-milling mixing method	35
Table 6. PIP sample measurements	42
Table 7. Knoop Hardness Results for PIP method	45
Table 8. Vickers Hardness results for precursor mixing method.....	53
Table 9. Ethanol mixing method sample measurements	58
Table 10. Preliminary Knoop Hardness Results for ethanol mixing method	63

LIST OF FIGURES

Figure 1. Major hazards in space environment.....	1
Figure 2. General PDC process with respect to temperature	6
Figure 3. General representation of the molecular structure of silicon-based polymers	8
Figure 4. Silicon-based polymers as precursors for ceramics.....	9
Figure 5. Weight loss of polysilazane precursor with and without thermal initiator.....	10
Figure 6. Molecular structure of silicon-based polymers before and after thermal decomposition	11
Figure 7. Linear shrinkage of SiCN precursor during pyrolysis.....	12
Figure 8. Density increase of SiCN precursor during pyrolysis	13
Figure 9. Different types of fillers and their effects on PDCs	15
Figure 10. Vickers hardness indentation and Knoop hardness indentation	17
Figure 11. Molecular structure of CNT and BNNT.....	18
Figure 12. Puffball BNNT: raw and refined	20
Figure 13. Calculated exposure to GCR of different shielding materials.....	23
Figure 14. different forms of reinforcements used in composites	24
Figure 15. Fundamental fiber mechanisms that occur while a crack extends through a CMC ...	25
Figure 16. CNT ceramic composites: crack deflection around CNTs along ceramic matrix, CNTs bridging gap between cracks, and CNT pullout.....	26
Figure 17. Increase in thermal conductivity for BNNT-SiCN composites at room temperature	29
Figure 18. Schematic for ball-milling mixing method.....	30
Figure 19. SEM surface view: control sample and 5 wt% sample	33

Figure 20. SEM cross section view: control and 15 wt%	33
Figure 21. SEM cross section view: ‘Damaged’ nanotubes (15 wt%)	34
Figure 22. Density and Hardness of BNNT-PDC.....	35
Figure 23. Illustration of PIP process to prepare CNT reinforced SiCN composites. a) CNT sheet, b) CNT/PSZ, c) CNT/SiCN1, and d) CNT/SiCN2.....	38
Figure 24. Mechanical properties of CNT-SiCN composites. a) Stress-strain curve and b) Young’s Modulus	39
Figure 25. Schematic for PIP method.....	40
Figure 26. BNNT mats submersed in precursor and exposed to vacuum.....	40
Figure 27. Quartz glass placed on top of composite mat to help prevent warping during heat treatment.....	41
Figure 28. Side view of BNNT-SiCN sample (28 wt%) with initial manufacturing method.....	41
Figure 29. Top view of BNNT-SiCN sample (35 wt%) with improved manufacturing method.....	42
Figure 30. SEM surface view of: BNNT mat and SiCN film.....	43
Figure 31. SEM cross section view of BNNT-SiCN (35 wt%)	44
Figure 32. SEM surface view of BNNT-SiCN (35 wt%)	44
Figure 33. Schematic for precursor mixing method	48
Figure 34. BNNT-PSZ solution time lapse: 0.1 wt% and 0.5 wt%	48
Figure 35. Rubber Mold and Teflon beaker.....	49
Figure 36. Cured precursor mixing samples removed from molds	50
Figure 37. BNNT-SiCN before and after pyrolysis	50
Figure 38. SEM surface view of BNNT-SiCN (0.1 wt%)	51

Figure 39. SEM surface view of BNNT-SiCN (0.5 wt%)	52
Figure 40. Schematic for ethanol mixing method.....	56
Figure 41. a) Ethanol mixed with preceramic powder and b) mixture with BNNT solution	56
Figure 42. Dried up powder mixture once ethanol has evaporated	57
Figure 43. Pressed powder samples (0, 1, 5, 10, 20 wt%, respectively) before pyrolysis.....	57
Figure 44. 1 wt% mixed powder: a) Ball-milling mixed powder and b) ethanol mixed powder	59
Figure 45. SEM image of 1 wt% ball-milling mixed powder.....	60
Figure 46. SEM image of 1 wt% ethanol mixed powder.....	60
Figure 47. SEM cross section view of ceramic 0 wt% sample.....	61
Figure 48. SEM cross section view of ceramic 1 wt% sample.....	61
Figure 49. SEM cross section view of ceramic 5 wt% sample.....	62

Chapter 1: Introduction

1.1 Space Environment

It has been over 50 years since the first manned mission to the Moon. The next major space exploration milestone is to send humans to Mars. The journey to Mars (one-way) is estimated to take about 7 months; quite lengthy compared to about 3 days to reach the moon. The mission to Mars crew, along with the spacecraft and equipment, will be exposed to the harsh environment of space for over a year. Space is a vacuum with numerous dangerous conditions such as micrometeorites and space radiation (Figure 1). The spacecraft will also experience a wide range of temperatures, both extremely hot and cold, during the mission. Designing the proper material to withstand the space environment for an extended period is critical for the safety of the astronauts and mission success.

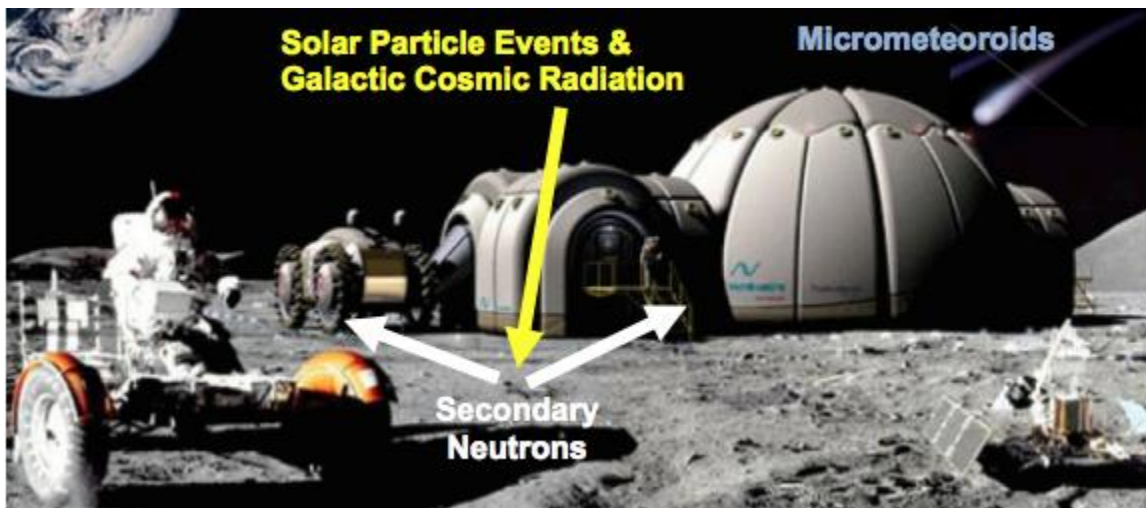


Figure 1. Major hazards in space environment [1]

Meteoroids are small rocky or metallic debris that drift through space at hyper-speeds that exceed 4-5 km/s and can be as high as 75 km/s [2]. Impacts at such speeds can cause significant damage or even destroy spacecraft. Micrometeoroids, meteoroids with a diameter of a few millimeters and a mass of less than one gram, can also cause a substantial amount of damage. It

has been estimated that a spherical 1 cm diameter meteoroid with a velocity of 1 km/s has the impact energy of a 30-caliber bullet and at 55 km/s has the impact energy of a hand grenade [2]. Sufficient shielding is required to withstand and protect the critical surfaces of the spacecraft from these high speed and high energy collisions.

The spacecraft must also survive the dynamic thermal environments during all phases of the mission. The spaceship will spend most of the mission in free space, which has an average temperature of 4 Kelvin [2], when traveling to and from Mars. Once at Mars, the space structures will have to endure the weather of Mars which ranges from 30 – (-140) °C and an average of -63 °C [3]. On the voyage back, the spacecraft will re-enter Earth's atmosphere which can cause the surface of a spacecraft to reach 1500 °C [4]. Therefore, it is important to design for these extreme temperatures and protect the outer layer of the spacecraft. Furthermore, it is important to generate and expel heat within the spaceship to maintain operating temperatures for components and subsystems.

On top of all these conditions, the spacecraft will constantly be exposed to space radiation. There are two primary sources of space radiation, galactic cosmic radiation (GCR) and solar particle events (SPEs). The GCR spectrum consists of about 87% hydrogen ions (protons), 12% helium ions (alpha particles) and 1-2% high charge and energy particles with atomic numbers between 3 (lithium) and 28 (nickel) [5]. The low atomic particles are easily shielded, but the heavier particles, like iron (26), can penetrate thick shields and cause significant damage. SPEs (or solar flares) emit millions of high-energy particles, mostly consisting of protons, over a short period of time and can produce a density flux of over 10^9 protons/cm² [5]. Low energy protons are easily protected by the spacecraft, but high energy protons (+30 MeV) will cause substantial harm without the proper shield. When GCR and SPE radiation interact with surfaces (such as a

spacecraft or regolith), a third source of radiation known as secondary neutrons are formed via nuclear collisions [5]. While secondary radiation only contributes to a small percentage of the overall radiation dose, it is important to minimize it as much as possible because it will accumulate over time (especially for lengthy deep-space missions).

1.2 Proposed Material

This work aims to develop a multi-functional polymer-derived ceramic reinforced with boron nitride nanotubes that can be integrated into current space technologies including entry, descent, and landing (EDL) systems, astronaut suits, and inflatable space structures. The ceramic matrix will be able to withstand the extreme temperatures and harsh conditions found in the space environment. The nanotube reinforcement will further improve the mechanical and thermal properties of the ceramic matrix along with the added benefit of providing neutron radiation shielding properties.

The polymer precursor used for all the experiments was polysilazane which transformed into SiCN ceramic material after thermal treatment. There are other types of polymer precursors that will create different compositions of ceramics such as SiC and SiCO. The precursor can be adjusted based on the application, but the composite manufacturing methods used in this research should be applicable with most polymer precursors.

1.3 Research Objectives

The objective of this research is to find an optimal manufacturing method for polymer-derived ceramics reinforced with boron nitride nanotubes. The polymer-derived ceramic route is very flexible and different techniques can be used to make composites. For each manufacturing method, the focus will be on the:

- i. BNNTs effect on the composite's dimensions (density, shrinkage, mass loss)

- ii. Dispersion of BNNT within the ceramic matrix
- iii. BNNTs effect on the composite's micro-hardness properties

The ultimate goal of this research is to design a multi-functional space material. The focus is to improve material properties for long-term space missions; in this case, the mission to Mars. In order to survive the harsh environment of space, the material must have the following properties:

1) Excellent toughness

When designing space suits or inflatable habitats, it is critical for the material to remain intact and undamaged. Materials with high toughness will protect these structures from potential breaches, e.g., from micrometeoroids, and minimize cracks after multiple cycles of use.

2) High thermal stability

The material must be able to withstand extreme temperatures without sacrificing mechanical properties. Space technologies will be exposed to both ends of the temperature spectrum, whether it be during the red-hot re-entry to Earth or inhabiting the frosty exterior of Mars.

3) Efficient neutron radiation shielding

Space radiation is one of the most dangerous hazards an astronaut will be exposed to during a lengthy mission. By having a structural material that can also shield neutron radiation, we can pack fewer shielding materials in the rocket and decrease the overall payload.

1.4 Thesis Outline

This thesis is divided into the following chapters:

Chapter 2 is the literature review of polymer-derived ceramics (matrix), boron nitride nanotubes (reinforcement) and composites. Chapters 3-6 will discuss the 4 different manufacturing methods used to create BNNT-PDC samples. Chapter 3 is the ball-milling mixing method. Chapter

4 is the polymer infiltration and pyrolysis method. Chapter 5 is the precursor mixing method. Chapter 6 is the ethanol mixing method. Chapter 7 will summarize the results from each method and discuss future work.

Chapter 2: Literature Review

2.1 Introduction to Polymer Derived Ceramics (PDCs)

Polymer-derived ceramics (PDCs) are synthesized by the pyrolysis (thermal treatment) of polymer precursors. The precursors represent inorganic/organometallic systems that allow the chemical composition and nanostructure of the ceramic to be controlled with proper heat treatment under an inert atmosphere [6,7]. PDCs are known for their advanced thermal-mechanical properties, such as their excellent oxidation and creep resistance at ultrahigh temperatures (up to 2000°C) [8]. Most PDCs follow a similar manufacturing process which consists of the following steps:

1. Synthesis of polymer precursors (0-100 °C)
2. Shaping and cross-linking of the polymer (100-400°C)
3. Polymer to ceramic transformation (400-1000°C)

The typical temperature ranges for each step are illustrated in Figure 2.

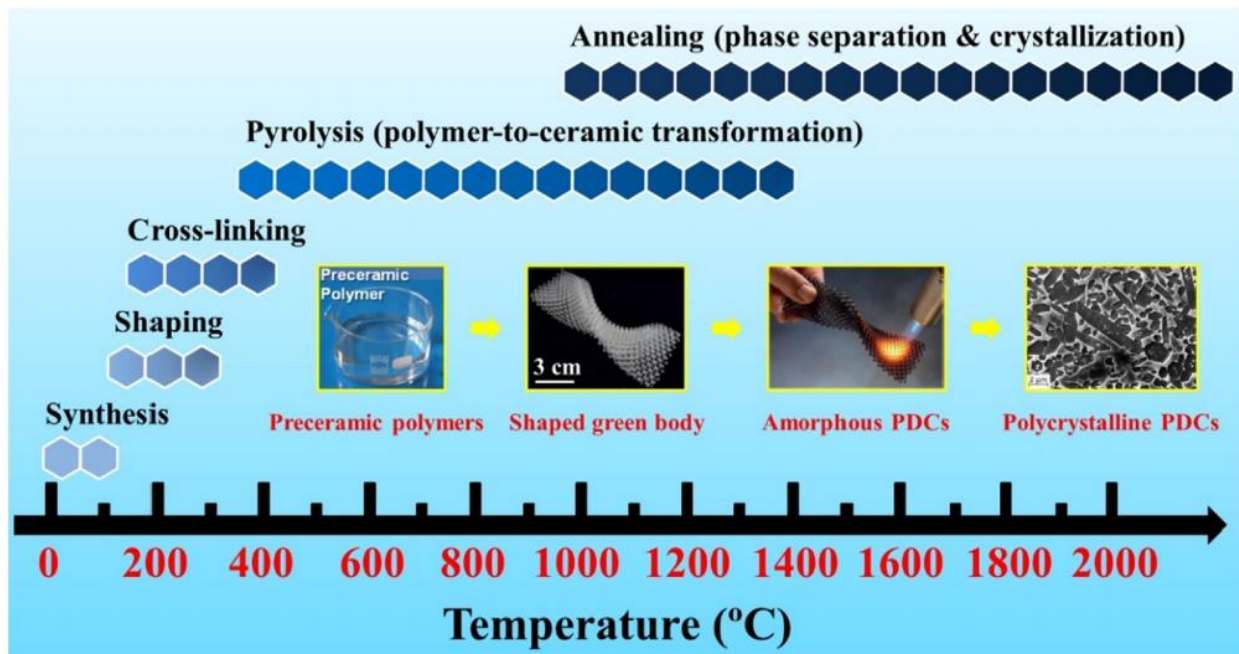


Figure 2. General PDC process with respect to temperature [9]

The PDC precursor route has many advantages over the traditional ceramic powder/slurry route. Traditional ceramic manufacturing is limited by the requirement of sintering additives, difficulty in creating complex shapes, and lower overall thermal stability when compared to PDCs [10]. The precursor route is more flexible and allows for different forms of ceramics to be formed such as ceramic fibers, layers, and composite materials. Polymer precursors can also be processed using polymer-forming techniques such as polymer infiltration pyrolysis (PIP), injection molding, coating from solvent, extrusion, or resin transfer molding (RTM) [8]. Once the polymer is fully shaped, it can undergo heat treatment to transform into a ceramic. Another advantage of PDCs is for complete ceramic transformation to occur at or below 1100°C [11,12], which is relatively low compared to traditional ceramics (1700-2000°C).

2.1.1 Polymer Precursor

The properties of PDCs are controlled by the chemistry of the polymer precursor. The molecular structure of the precursor directly influences the composition, microstructure and phase distribution of the final ceramic [13]. Therefore, selecting the proper precursor for the application is very important. Creating successful silicon-based PDCs is heavily dependent on the bonding strength between silicon and carbon in the precursor. The bonding strength prevents the volatilization of small hydrocarbon molecules during pyrolysis in an inert atmosphere [13,14]. The ideal precursor should have the following properties to be effective at thermal decomposition [13]:

- High molecular weight to avoid volatilization of low molecular weight components
- Sufficient viscoelasticity and solubility for the shaping process
- Presence of functional groups in order to gain thermosetting and curing properties
- Cage or ring polymeric structures to reduce volatilization

The general formula of silicon polymers can be seen in Figure 3. Different silicon polymers can be designed by modifying the (X) group of the polymer backbone or by varying the R¹ and R² substituents attached to the silicon [13]. Different classes of silicon-based polymers can be created by varying the X group such as the following:

- Poly(organosilanes) when X = Si
- Poly(organocarbosilanes) when X = CH₂
- Poly(organosiloxanes) when X = O
- Poly(organosilazens) when X = NH

These silicon polymers and more can be seen in Figure 4. While the X group controls the chemical composition of the final ceramic, modifying the R substituents can change different ceramic properties such as chemical/thermal stability, electronic, optical, and rheological properties. Also, the R side groups control the carbon content present in the final product. For this research, Polysilazane will be used. Its chemical composition can be seen in Figure 4 and after pyrolysis it will transform into amorphous SiCN.

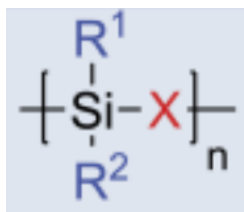


Figure 3. General representation of the molecular structure of silicon-based polymers

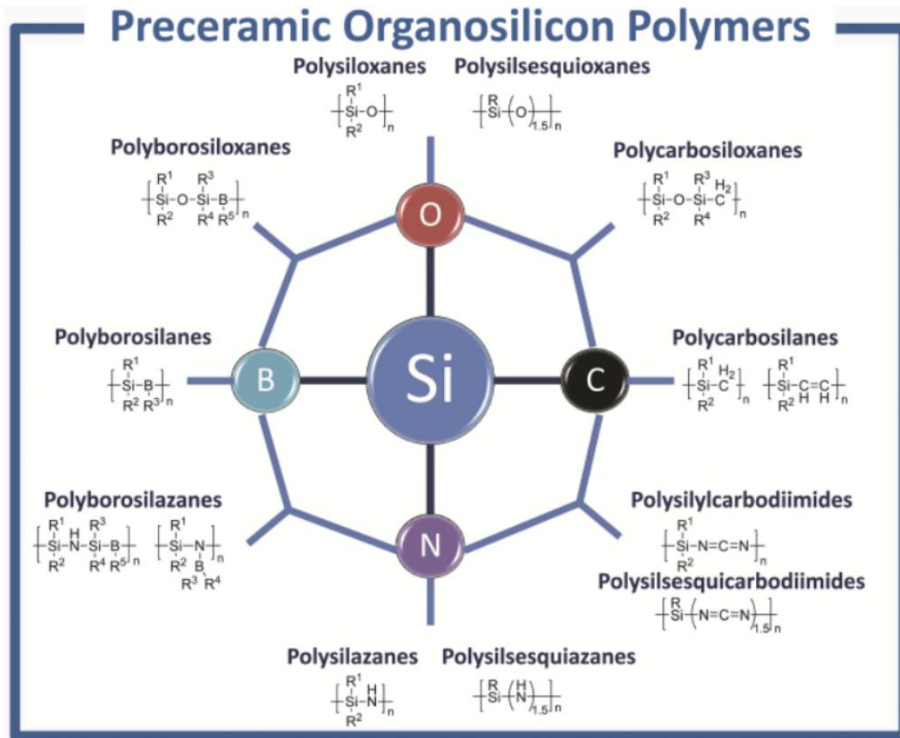


Figure 4. Silicon-based polymers as precursors for ceramics [8]

2.1.2 Curing: Polymer Shaping and Cross-linking

Traditional ceramics are typically shaped with the following methods: dry pressing, plastic forming, slip casting and pressure casting [15]. These methods are limited by the size and geometric complexity of the final product, as well as the need for large and expensive equipment. On the other hand, preceramic polymers have a vast number of shaping techniques and include the following [8]:

- Casting
- Infiltration
- Coating
- Pressing injection molding
- Extrusion
- Fiber drawing
- Foaming
- Machining
- Joining
- Ink jetting
- Aerosol spraying
- Etc.

Polymer precursors have also been used to make ceramic matrix composites. These composites are typically made via the polymer infiltration and pyrolysis (PIP) method, which has been shown to be quicker and better for the environment when compared to the chemical vapor infiltration method [16].

Once the polymer is shaped, it must be able to maintain its shape during pyrolysis. This can be achieved by using a precursor that is either a cross-linkable liquid or curable solid. Cross-linking helps prevent oligomers and low molecular weight polymers from volatilizing during pyrolysis. Certain functional groups, such as Si-H, Si-OH and Si-vinyl, cause condensation and addition reactions to take place, which cause the precursor to thermoset (become unmeltable or insoluble) [17-20]. Most precursors cure around 200°C but this temperature can be lowered by using a thermal initiator, which helps prevent oligomers from evaporating thus decreasing the formation of bubbles and increasing the ceramic yield [21,22]. Figure 5 shows the effect of using a thermal initiator. Another method to prevent pores from forming is a unique pressure casting technique where the liquid precursor is cured under pressure [23].

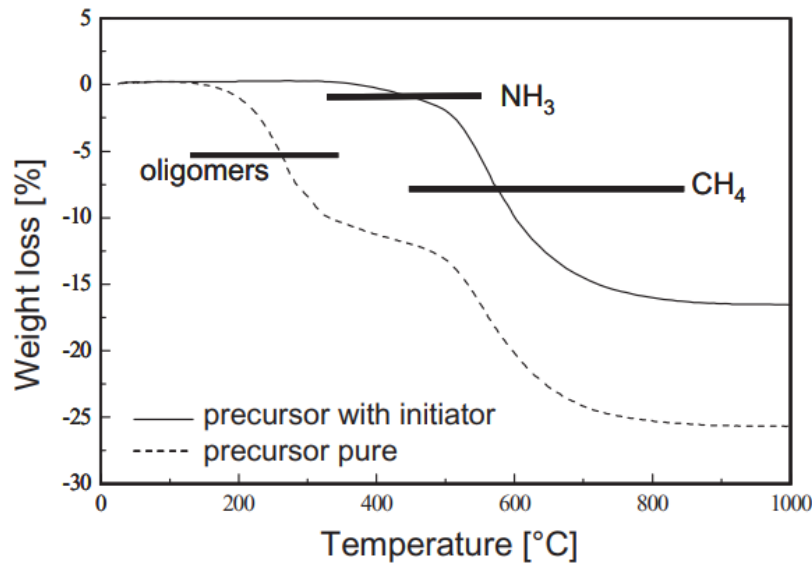


Figure 5. Weight loss of polysilazane precursor with and without thermal initiator [24]

2.1.3 Pyrolysis: Polymer to Ceramic Transformation

Once cured, the polymer can undergo further heat treatment above 300 °C (commonly known as pyrolysis) to begin the ceramic conversion. During this transformation, many chemical reactions occur causing chemical bonds to split, new bonds to form, and organic groups, such as methane, benzene, methylamine, ammonia, and hydrogen, to be removed [18,19]. Figure 6 shows a few examples of the molecular structure transformation caused by pyrolysis.

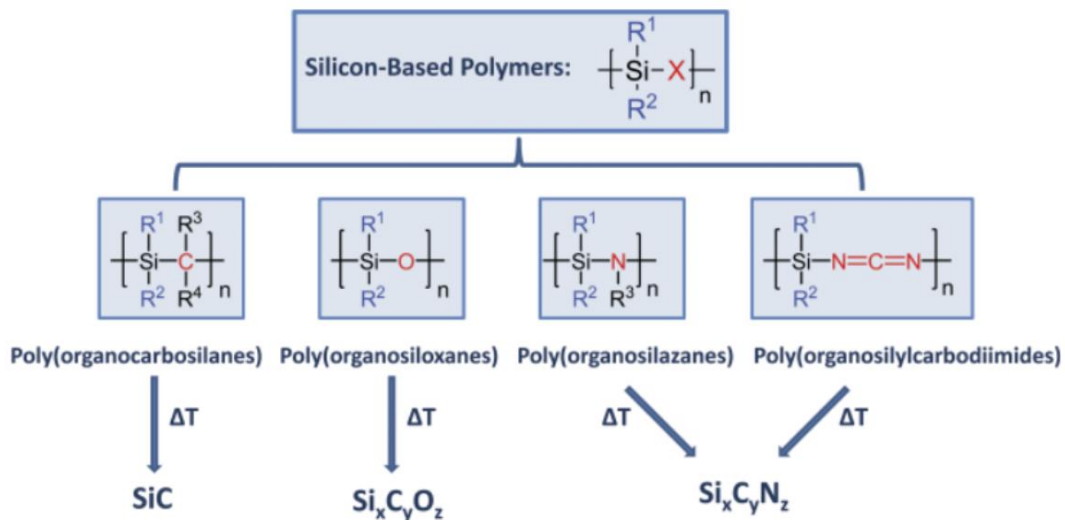


Figure 6. Molecular structure of silicon-based polymers before and after pyrolysis [8]

Pyrolysis is typically performed in an oven or furnace with a constant flow of gas (usually inert) to help remove the decomposition gases [25,26]. With Polysilazane, amorphous SiCN ceramic is formed at around 1000°C, and if further heat treatment is added the ceramic will start to crystallize at around 1600°C. However, for most applications, crystallization is not needed or desirable and heat treatment is halted once the ceramic is amorphous [27].

During pyrolysis, the precursor will shrink significantly (up to 20%). This is one of the major disadvantages of the PDC route when compared to traditional ceramic sintering. This shrinkage is caused by two main effects. The first is due to the precursor losing a significant

amount of weight because during this process many organic and inorganic groups are being removed. The second is caused by the chemical bond rearrangement of Si, C and X groups into more dense networks. This substantial amount of volume shrinkage leads to an increase in overall density. Figures 7 & 8 show the linear shrinkage and density increase of a SiCN precursor during pyrolysis, respectively. Another disadvantage is the formation of pores within the matrix during thermal treatment. If the gases formed during pyrolysis are not properly removed from the matrix, they will remain as pores in the final product.

This research will stop at the amorphous phase because there will be less shrinkage and smaller pores compared to the crystalline phase. This will help lower the amount crack formations and decrease internal stresses that could lead to failure.

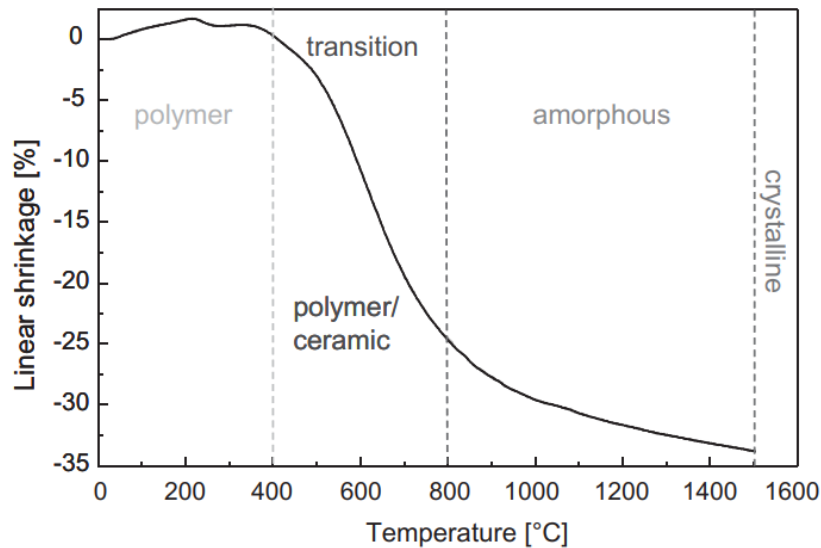


Figure 7. Linear shrinkage of SiCN precursor during pyrolysis [24]

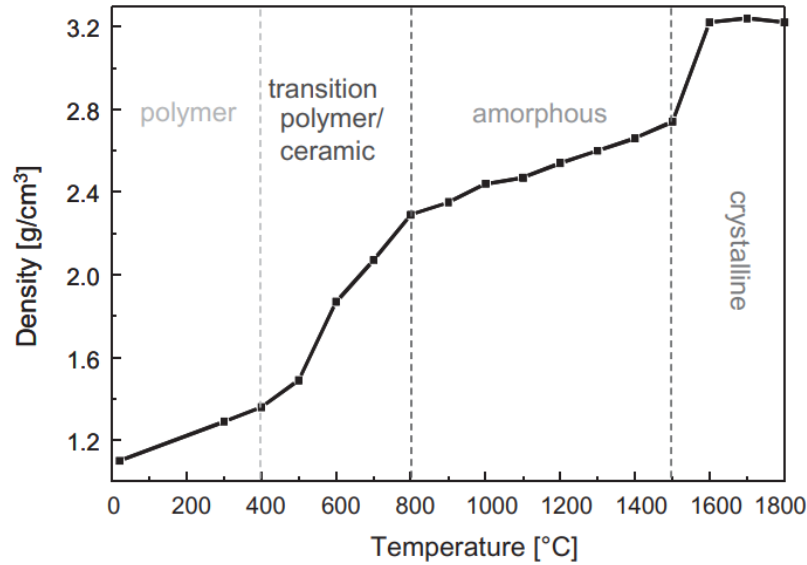


Figure 8. Density increase of SiCN precursor during pyrolysis [24]

2.1.4 Fillers

As previously mentioned, one of the biggest drawbacks of the PDC route is the volume shrinkage (20-30%) and introduction of pores during the polymer to ceramic transformation. Fillers can be added during the polymer phase to combat against shrinkage. Fillers come in various forms (polymeric, ceramic, metallic) and dimensions (nano/micro powders, platelets, nanotubes) [8]. There are four main types of fillers (Figure 9) used for PDCs:

1. Passive fillers
2. Active fillers
3. Meltable fillers
4. Sacrificial fillers

Passive fillers are inert and do not react with the preceramic polymer during thermal treatment. Their main purpose is to reduce shrinkage and prevent cracks/large pores from forming by providing an escape route for the gases generated during pyrolysis [28]. Some fillers only remain inert during certain conditions such as low temperature or inert atmosphere. This may be

hard to achieve with the harsh environment created during pyrolysis. Therefore, passive fillers are typically ceramic materials because pyrolysis can damage polymers, melt glasses, and oxidize metals [13]. While passive fillers help reduce shrinkage during the ceramic transformation, they will not reduce porosity. Porosity can increase if too much passive filler is used, especially if the filler has a narrow particle size distribution [29]. Although overall shrinkage is reduced, cracks may still form due to localized stresses around the filler particles [30,31].

Active fillers will cause chemical reactions during heat treatment of the PDCs. These fillers help prevent shrinkage by expanding at high temperatures. Some researchers have estimated the amount of volume-expanding filler needed to cause zero shrinkage during the polymer to ceramic transformation phase [29,32,33]. Active fillers can also introduce new phases to the PDC, which can be used to alter certain ceramic properties. Furthermore, some fillers can completely change the chemical composition of the final product when added to the precursor [34,35]. Most active fillers are either metallic or semi-metallic, especially those that contain Si, B, Al and transition metals from groups 4 to 6 on the periodic table [13,36,37].

Meltable fillers are usually glasses because they will melt or soften at high temperatures. This allows the glass to fill up the ceramic pores and increase overall density, which has shown improvements against oxidation and corrosion [38,39]. It is important to note that these fillers can act as active fillers because they can react with other components in the system [40]. Using meltable fillers correctly requires proper precursor selection and sufficient heat treatment. If the temperature is too high, the glass could crystallize or decompose. If the temperature is too low, the glass may not melt or soften enough, and it will behave like a passive filler.

Sacrificial fillers are mostly organic compounds added to the precursor and removed from the system by either by thermal decomposition or by using a solvent. This allows the ability to

generate and control porosity in the PDC. This strategy has been used before in gas separation membranes [41-43]. The porosity type, amount, size and distribution can be controlled in the PDC by selecting the proper organic filler.

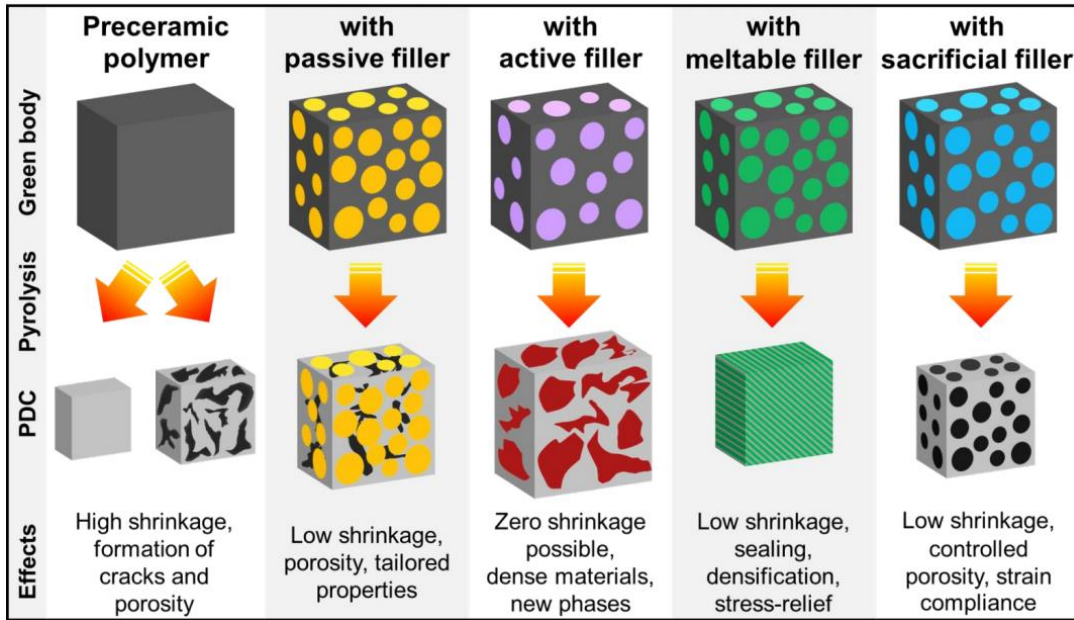


Figure 9. Different types of fillers and their effects on PDCs [30]

2.1.5 Mechanical Properties of PDCs

The study of the mechanical properties on bulk pristine PDCs has been limited due to the difficulty in creating large, fully dense, and crack-free bulk specimens. Two methods have been utilized to make small dense bulk samples. The first is the powder route which involves ball-milling partially cured precursor into powder, pressing the powder into a compact and then perform pyrolysis [44,45]. The second is the liquid route which is based on casting either a sol-gel solution or liquid polymer into small cylinders or thin plates for flexural and fracture mechanical tests [46,47]. Table 1 compares different mechanical properties from various commercially available SiCN precursors. For this research, SiCN (Ceraset) was used.

Table 1. Mechanical properties of bulk Si-C-N systems [8]

System	Bulk Density (g/cm ³)	Elastic Modulus (GPa)	Vickers Hardness (GPa)
SiCN (Ceraset)	1.85-2.16, 2.3	82-140 155	8.3-11.3 15-26
SiCN (NCP200)	2.32	110-130	11-15
SiCN (VT50)	1.95	105	6.1
SiCN (HVNG/HPS)	2.6	109-118	7.9-12.8

Hardness (H) is a material's ability to resist plastic deformation and can be used to measure a ceramic's mechanical strength on the microscopic scale. This property is calculated by applying a load (P) to a material via a geometrically defined indenter and dividing it by the indentation area (A). The simplified hardness formula can be seen below along with the general form which includes a constant based on indenter geometry (β) and length of the indentation (d).

$$H = \frac{P}{A} = \beta \frac{P}{d^2}$$

Micro-hardness measurements are favorable for bulk PDCs because only a small specimen is required and the test will not destroy the sample. There are multiple micro-hardness tests each with a uniquely shaped indenter, but Vickers and Knoop are the most common for testing ceramic hardness [48]. Vickers hardness has a diamond-shaped indenter and has a β value of 1.8544. While Knoop hardness has a wide diamond-shaped indenter and has a β value of 14.229 [49]. The shape of the Vickers and Knoop indentations can be seen in Figure 10. Vickers hardness is recommended for thick samples (bulk material) with a large amount of surface area, and Knoop is recommended for thinner samples (thin layers or coating). Vickers and Knoop values are typically reported as

unitless but they technically have units of kgf/mm^2 . To convert these unitless values into pascals simply multiply by gravity (9.807) to yielding MPa. For this research, I will report both the unitless and pascal hardness values.

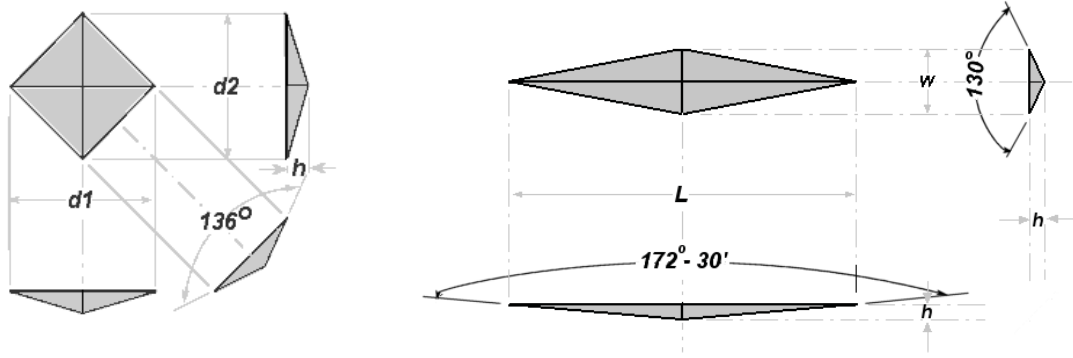


Figure 10. Vickers hardness indentation (left) and Knoop hardness indentation (right) [50]

2.2 Introduction to Boron Nitride Nanotubes (BNNTs)

Boron nitride nanotubes (BNNTs) are a relatively new type of nanomaterial with incredible properties. BNNTs are rolled-up cylinders of hexagonal boron nitride (h-BN) sheets with alternating B and N bonds [51]. They have a diameter of a few nanometers and their length can range from 100 nm to a few microns, which allows them to have very high aspect ratios (< 1000).

BNNTs are analogous to carbon nanotubes (CNTs) because they share a similar molecular structure (Figure 11) and mechanical properties. Both were discovered around the same time over 25 years ago. CNTs were first synthesized in 1991 by Lijima using an arc-discharge evaporation method [52]. Since their discovery, nanotubes have been researched heavily because of their unique structural features and incredible properties [53]. A few researchers proposed that boron nitride nanotubes could be formed based on the similarities in properties between carbon and boron-nitride materials [54]. In 1995, Chopra et al. were able to successfully synthesize BNNTs using a plasma arc discharge method [55].

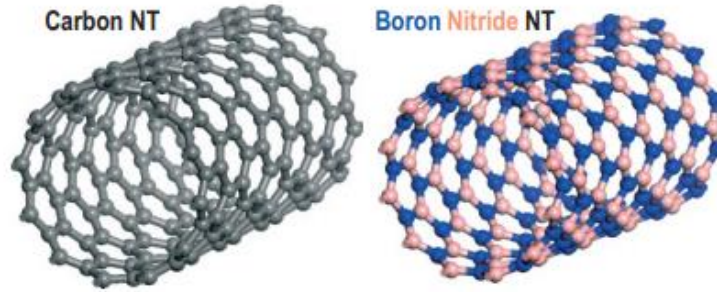


Figure 11. Molecular structure of CNT and BNNT [56]

Different properties of CNT and BNNT can be seen in Table 2. Both share similar mechanical properties, but BNNTs have unique properties that are attractive for space applications, such as their thermal stability (up to 900°C) in air which is twice as high as CNT (up to 400°C). Additionally, BNNTs can shield against neutron radiation due to its very high neutron absorption cross-section. This shielding property will be discussed further in section 2.2.3. BNNTs are also piezoelectric (ability to convert mechanical stress into electric charge and vice versa) which is caused by polarization due to the alternating placement of the boron and nitrogen atoms [57].

Table 2. CNT and BNNT properties [51]

	Carbon nanotubes	Boron nitride nanotubes
Constituent elements	C	B and N
Mechanical property	Elastic modulus 1.3 (TPa); Strength >65 GPa	Elastic modulus 1.18 TPa
Electrical properties	Metallic: ballistic conductor, ampacity $>10^9$ A cm ⁻² (>copper) Semiconducting: high mobility, band gaps about 0.5–2 eV	Wide bandgap semiconductor larger than 6.0 eV
Thermal conductivity	>3000 W m ⁻¹ K ⁻¹ at 25 °C (>diamond)	High value expected, but lower than CNTs; minimal data
Optical properties	Strong absorption across the entire spectrum; NIR fluorescence	Transparent in visible and infrared regions; Absorption in UV region
Thermal oxidation resistance	Stable up to 400 °C in air	Stable up to 900 °C in air
Neutron absorption cross-section	C: 0.003 barns	B: 767 barns (¹⁰ B ~ 3800 barns) N: 1.9 barns
Appearance colour	Black	White or slightly beige

2.2.1 BNNT Manufacturing and Quality

Although BNNTs have incredible properties for space applications, it is quite difficult to produce high quality BNNTs at a large scale because of the extreme conditions, such as high temperature and pressure, necessary during the manufacturing process. Only recently have a few manufacturing methods proven to make high quality BNNTs in the gram-scale quantity. These methods include the ball-milling/annealing method, the chemical vapor deposition (CVD) method, the high-temperature pressure (HTP) method, the hydrogen-assisted boron nitride nanotube synthesis (HABS) method, and the extended-pressure inductively-coupled plasma (EPIC) method [51].

The BNNTs used in this research were manufactured using the HTP method and were purchased from BNNT, LLC (Newport News, VA). Different forms of BNNT can be purchased from this vendor, such as puffball, thin paper, and powder. Figure 12 shows the 2 types of puffball BNNTs, raw and refined, available from the vendor. The raw form contains high quality nanotubes, but it is accompanied with many impurities (~50%), such as elemental boron (which causes the dark grey color). The raw BNNT can be treated using a proprietary purification method, which removes almost all impurities (less than 1% remains) and gives the BNNT a white color, to create refined BNNT. For this research, raw BNNT puffball were purchased due to their lower cost and readily availability compared to the refined BNNT. The current average price for raw puffball BNNT from BNNT, LLC is about \$700/gram.



Figure 12. Puffball BNNT: raw (left) and refined (right) (from BNNT, LLC website)

The HTP method uses a laser beam to heat up a boron source in a pressurized chamber with a nitrogen atmosphere. The laser heats up the boron to its vaporization temperature (~ 4000 K) and the nitrogen gas is pressurized to 0.7-1.4 MPa. The hot boron vapor rises and interacts with a cooled metal wire, which causes condensation and creates boron droplets. These droplets then act as a nucleation site and allow the boron to interact with nitrogen gas to form BNNTs. The BNNTs will continue to grow and cluster together to make a long continuous fibril. The HTP method was able to create high quality BNNTs with small diameters (< 5 nm), extreme length ($\gg 1000$ aspect ratio), small number of walls and few defects [58,59]. This method was developed by NASA Langley Research Center, in collaboration with the National Institute of Aerospace (NIA) and the Jefferson Science Associates (JSA).

2.2.2 BNNT Paper (mat)

BNNTs can be shaped into different assemblies (such as thin films, yarns, and paper) to maximize their incredible properties in real-world applications. BNNT paper (or mat) is a non-woven freestanding nanotube sheet with high porosity and a thickness of about $100 \mu\text{m}$. These papers are very desirable because they can be easily integrated in ceramic, metal, and polymer

matrices to create high-performance composites [60]. Without BNNT paper, the raw BNNT would have to be dispersed in the matrix, which could yield lower weight percentages and non-uniform distribution.

BNNT paper is very similar to CNT paper (also known as buckypaper). It is important to note that the term ‘buckypaper’ by itself refers to CNT paper, but it can also be used to describe BNNT paper, i.e., BNNT buckypaper. The most common technique for creating both CNT and BNNT paper is vacuum filtration. The first step is to disperse the nanotubes in a solvent, typically water, along with a surfactant, Triton X-100 (for CNTs) [61,62] or CTAB (for BNNTs) [63]. Nanotubes are prone to forming bundles and aggregates because of their high surface area and strong van der Waals interactions. The surfactant along with some form of mixing (either sonication or mechanical stirring) helps break up these clusters and allows the nanotubes to be fully dispersed in the solution. The homogenous solution is then vacuum filtered using a Teflon or nylon filter with sub-micron sized pores. During the filtration, the nanotubes are deposited on the filter surface and form a thin nanotube sheet (nanotube paper). Currently, BNNT mats are in the early stages of development. They contain many impurities and the nanotubes within the mat are not aligned. Further research is required to optimize BNNT mats.

2.2.3 BNNT Neutron Shielding Ability

Material selection is critical when designing a shield to protect against ionizing radiation. Studies have shown that the lower the atomic number of the shielding, the more effective it will be. Lower atomic numbers will have smaller fragmenting particles when interacting with radiation (which means less damage). Therefore, hydrogen is theoretically the best element for radiation shielding [64]. The current standard material for shielding space radiation is Polyethylene (C₂H₄)_n thanks to its high hydrogen content. Polyethylene is an excellent radiation shielding material, but

it is not a strong structural material [65]. For future space missions it would be ideal to have both the structural and shielding properties combined into one multi-functional material.

BNNTs can shield neutrons due to their boron content. The boron can slow down high energy radiation and since boron and nitrogen have low atomic numbers, less fragmentation of the shielding material will occur. A shield's neutron shielding effectiveness can be estimated by the material's neutron capture cross section. This is the probability of a neutron interacting with a target nucleus and is typically measured in barns ($1 \text{ barn} = 10^{-24} \text{ cm}^2$). The larger the cross section, the more likely the neutrons will interact with the nucleus. Natural boron has a high neutron capture cross section (767 barns) compared to most materials, for example nitrogen only has about 2 barns. This shielding can be improved by using Boron-10 isotopes when fabricating the nanotubes. Boron-10 has a very high neutron capture cross section (3800 barns) which allows it to absorb and slow down secondary neutrons more effectively.

The BNNT's shielding capabilities can be improved further by using a chemical treatment process known as hydrogenation. This process will add hydrogen to the nanotubes. Studies have also shown hydrogenated BNNTs having the ability to shield against radiation found in GCR [1]. Figure 13 shows BNNT with 5 wt% hydrogen (BN+5%H) outperforming Polyethylene (PE). Hydrogenated BNNTs (enriched with B-10) would be ideal for protecting against space radiation. The B-10 isotope would shield against secondary neutrons, while the hydrogen will slow down GCR and SPE radiation.

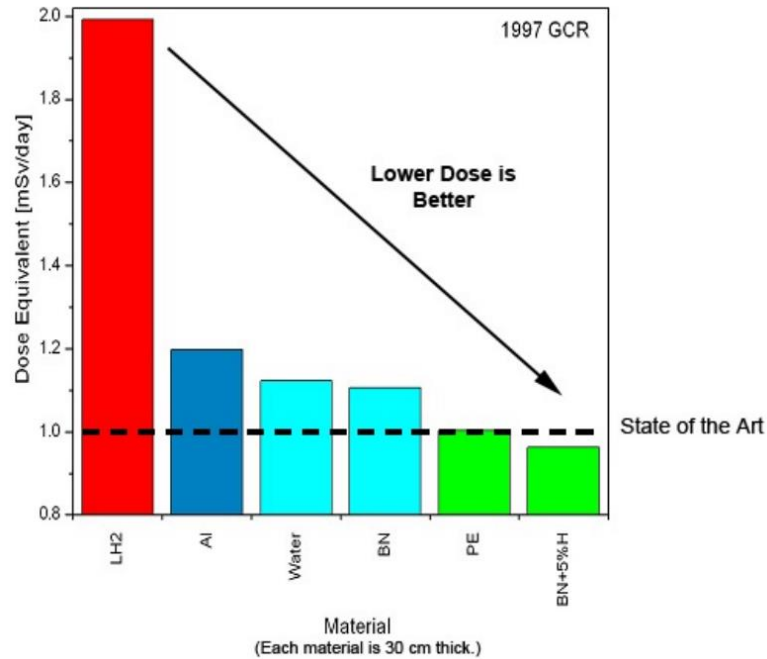


Figure 13. Calculated exposure to GCR of different shielding materials [1]

2.3 Introduction to Composites

A composite is a material with two or more components that have different physical or chemical properties. By combining materials with different properties, it is possible to make a new material with all the benefits of the individual components. The main advantage of composites is their improvement in mechanical properties while maintaining a low density compared to bulk materials. Composites are composed of matrices and reinforcements.

The matrix is the continuous phase that houses and protects the reinforcement. It also helps distribute the load. There are three main types of composites and they are usually categorized by their matrix – polymer matrix composites (PMC), ceramic matrix composites (CMC) and metal matrix composites (MMC). The reinforcement is the distributed phase and contributes the main strength to the composite. Reinforcements can come in various shapes and sizes, such as particles, fibers, and laminates (Figure 14).

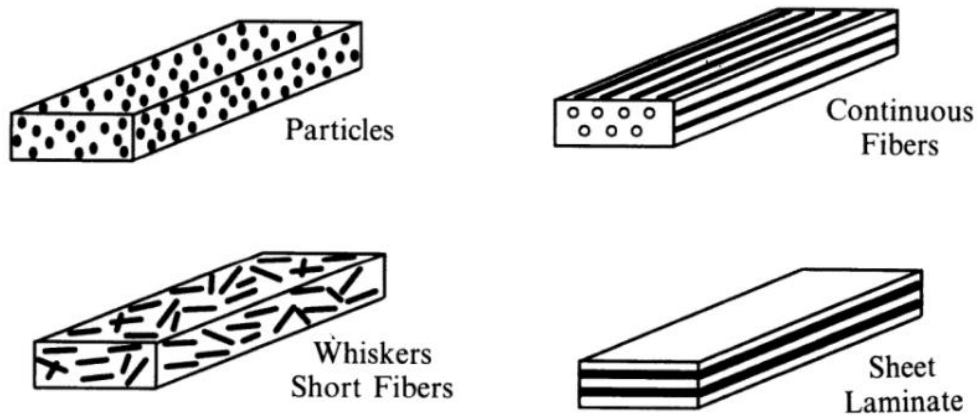


Figure 14. different forms of reinforcements used in composites [66]

2.3.1 Ceramic Matrix Composites (CMCs)

CMCs are exceptional candidates for structural applications because of their excellent strength and toughness at high temperatures all while maintaining a low density. They perform better than traditional ceramics which have disadvantages such as low fracture toughness, brittleness, and limited thermal shock resistance [67]. Preceramic polymers are used to manufacture CMCs in two different ways: by creating ceramic fibers to use as reinforcement or by creating the ceramic matrix using the polymer infiltration and pyrolysis (PIP) technique. The PIP process will be discussed further in Chapter 4. This literature review will focus on fiber and nanotube reinforced ceramics.

A wide variety of fibers have been used to create CMCs, these include SiC, carbon, alumina, and mullite [68-70]. Carbon fibers have shown some of the highest mechanical improvements and have been used to reinforce ceramics matrices since the 1960s [71]. Major improvements to fracture toughness for both carbon- and SiC-fiber-reinforced CMCs when compared to the pristine ceramic have been reported [72-74]. Fibers can toughen composites due

to various fiber mechanisms such as fiber debonding, fiber pull-out, and crack bridging [75]. These mechanisms are displayed in Figure 15.

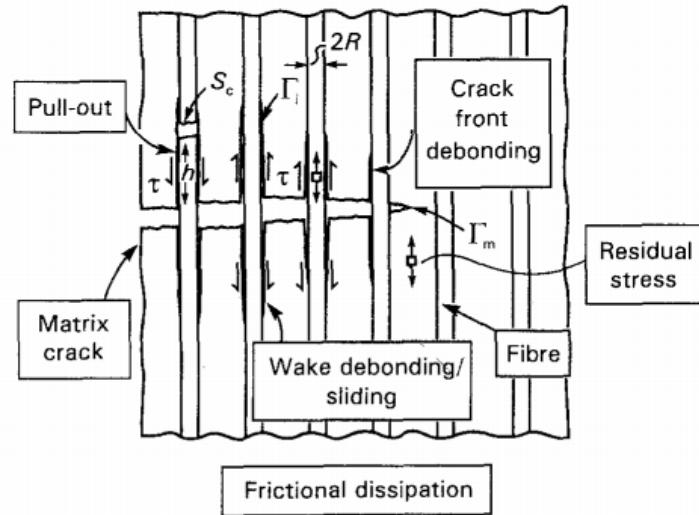


Figure 15. Fundamental fiber mechanisms that occur while a crack extends through a CMC [75]

Carbon nanotubes (CNTs) have received a massive amount of attention in recent years because of their extraordinary properties and could be seen as an evolution of carbon fibers. Most CNT composites have been concentrated on polymer matrices [76] but there have been a few CNT reinforced CMCs. In 2003, Xia et al. were able to report the first evidence of the toughening mechanisms of CNTs in a ceramic matrix [77]. With the CNT ceramic composites, they were able to demonstrate the three mechanisms of toughening found in fiber composites: crack deflection at the fiber/matrix interface, crack bridging, and fiber pullout (Figure 16). These features allowed the composite to resist more deformation thus causing an increase in both toughness and yield strength when compared to the porous pristine ceramic.

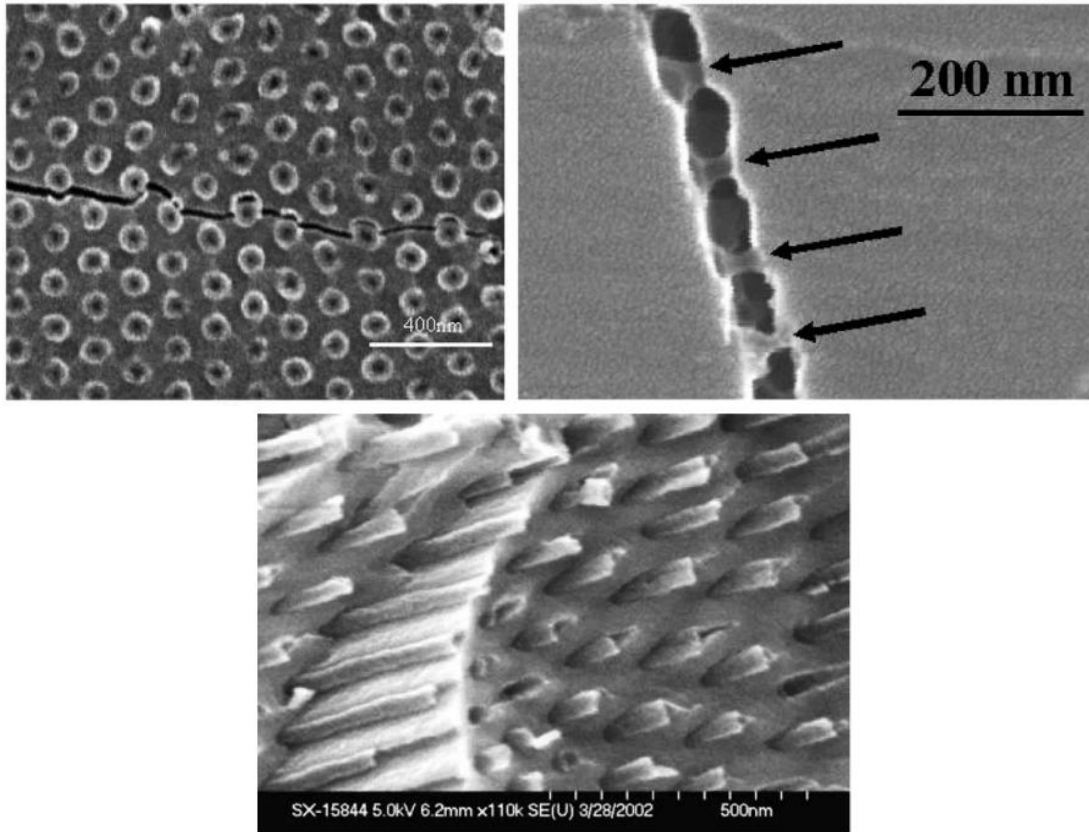


Figure 16. CNT ceramic composites: (top left) crack deflection around CNTs along ceramic matrix, (top right) CNTs bridging gap between cracks, and (bottom) CNT pullout [77]

2.3.2 BNNT Reinforced Composites

Most BNNT composites consist of BNNTs being integrated into a polymer matrix. Many researchers have used BNNTs as reinforcements for polymers such as polycarbonate, polystyrene, polyurethanes, and epoxy resin to increase mechanical properties [78-83]. In these studies, researchers reported an increase in elastic modulus (10-50%) with composites containing 1-5 wt% BNNT. Only a limited amount of BNNT metal composites have been published. One study used BNNT to reinforce a titanium matrix composite using a cold-press and sintering method [84]. The titanium composite with 4% volume BNNT was able to increase compressive strength by 145% compared to the pristine titanium.

There have been a few reports on BNNT ceramic composites with alumina, silicon nitride, and barium calcium aluminosilicate glass as the ceramic matrix [82,85-87]. Table 3 shows the Vickers hardness results for aluminum oxide and silicon nitride BNNT composites. The aluminum with 0.5 wt% BNNT was able to increase hardness by 13.9% while the 2.5 wt% BNNT sample decreased hardness by 16.2%. This suggests maybe only a small amount of BNNT is required to improve mechanical properties in ceramics. The silicon nitride with 0.5 and 5 wt% BNNT were not able to increase hardness when compared to the pristine ceramic. It important to note that the ceramics from these hardness results were made with traditional powder sintering techniques and not the polymer derived technique. Very little work has been published on the mechanical properties of BNNT polymer-derived ceramic composites.

Table 3 Sintering conditions and mechanical properties of BNNT ceramic composites [86]

Materials	Sintering conditions			Mechanical properties	
	Temperature (°C)	Duration (min)	Relative density (%)	Vickers hardness (GPa)	Young's modulus (GPa)
Al ₂ O ₃	1500	3	100	17.3 ± 0.6	400
0.5 wt% BNNT/Al ₂ O ₃	1500	3	98.2	19.1 ± 0.7	379
2.5wt% BNNT/Al ₂ O ₃	1500	3	97.1	14.5 ± 0.5	359
Si ₃ N ₄	1600	5	98.5	18.3 ± 0.3	300
5 wt% BN _p /Si ₃ N ₄	1750	5	99.5	11.8 ± 0.8	249
5 wt% BN _n /Si ₃ N ₄	1650	5	98.2	15.1 ± 0.7	243
0.5 wt% BNNT/Si ₃ N ₄	1600	5	97.3	15.5 ± 0.6	273

Chapter 3: Ball-milling Mixing Method

3.1 Introduction

Manufacturing bulk ceramic samples with the polymer precursor in liquid form is quite difficult because of the large amount of gas that is released during pyrolysis. The gases formed within the center of the material have no path to exit and will form bubbles which can lead to crack formation. This issue can be avoided by curing the polymer precursor and ball-milling the cured product to form powder. The powder is then pressed into the desired shape to form a compact. The compact then undergoes pyrolysis to form the ceramic. The powder route introduces porosity in the compact and allows for the gases to be removed from the system. During pyrolysis, most of this porosity will disappear due to the natural shrinkage that occurs with PDCs during heat treatment. This technique has been used to create amorphous and crack-free ceramics with relative densities up to 93% [44].

The ball mixing method was used to create the first set of bulk BNNT-SiCN composites. The polymer precursor was cured and ball milled to form powder. BNNT puffball and cured powder were then mixed using additional ball-milling. This powder mixture was pressed in a circular die and then underwent pyrolysis to form the ceramic composite. This method allowed us to successfully manufacture BNNT-SiCN composites with different weight percentages of BNNT (0, 5, 10, 15, 20, 25 wt%). These composites had an average diameter of about 12 mm and average thickness of about 1.5 mm.

We investigated the thermal properties of these samples and published the findings [88]. The most notable result was the 2100% increase in thermal conductivity at room temperature with the 25 wt% composite when compared to the pristine ceramic (Figure 17). Please note that the 20 wt% sample was not used for the thermal conductivity test because it was required for another

experiment. The results published proved one can increase the thermal properties of the ceramic matrix by adding BNNTs. Thus, allowing us to achieve one of the main objectives of this research for developing multi-functional composites for space applications.

In this chapter, I plan to discuss the mechanical properties of the composites made with this method, along with the BNNT dispersion and the effects BNNTs have on the ceramic matrix.

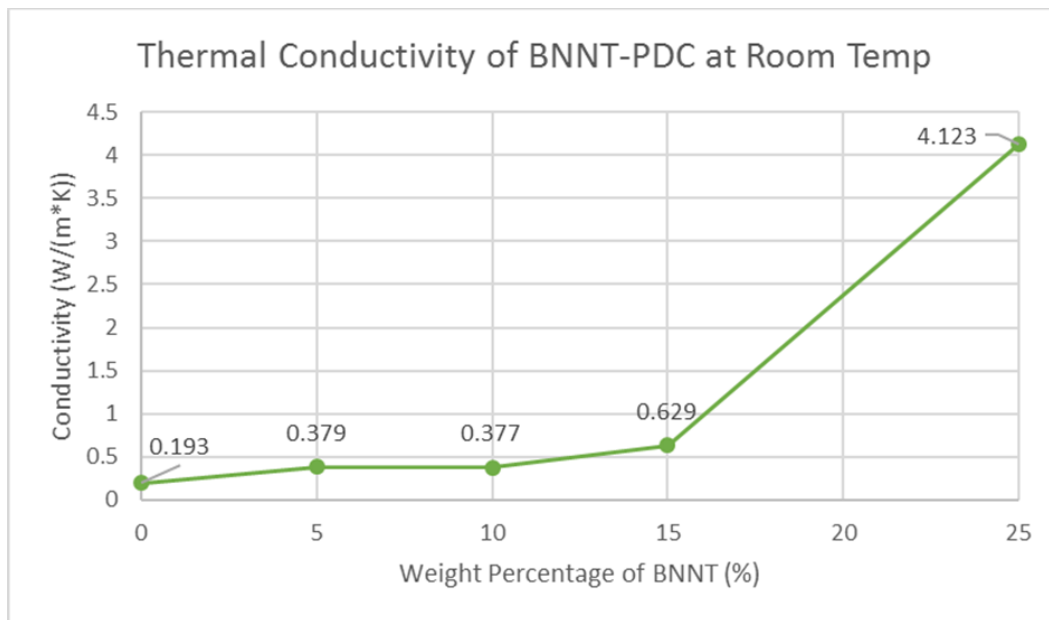


Figure 17. Increase in thermal conductivity for BNNT-SiCN composites at room temperature

3.2 Experimental

Figure 18 illustrates the steps used to make composites with the ball-milling mixing method. Polysilazane (PSZ, KiON Defense Technologies, Inc., Huntingdon Valley, PA), the polymer precursor, was mixed with 4 wt% dicumyl peroxide (thermal initiator) and cured at 150 °C in a tube furnace with an argon atmosphere. Once cured, the solid cross-linked polymer was ball milled for 1.5 hours to form PSZ powder (size ~1 μm). After the powder finished with its first phase of ball-milling, the BNNT puffball (from BNNT, LLC, Newport News, VA) was added to the powder. The BNNT and PSZ powder were mixed using the ball-milling machine for 30

minutes. The mixed powder was collected and prepared for cold pressing. Two drops of liquid precursor were added to the powder to help with binding during the press. The powder mixture was placed in a 14.85 mm circular die and pressed with 34 MPa of uniaxial pressure to form the powder compacts. Each press used 0.3 grams of powder. The compacts underwent pyrolysis at 1000°C for 3 hours with a ramp up rate of 1 °C/min in a nitrogen atmosphere to form the BNNT-SiCN samples. A total of 6 different samples were made with this method: 0, 5, 10, 15, 20, 25 wt% of BNNT.

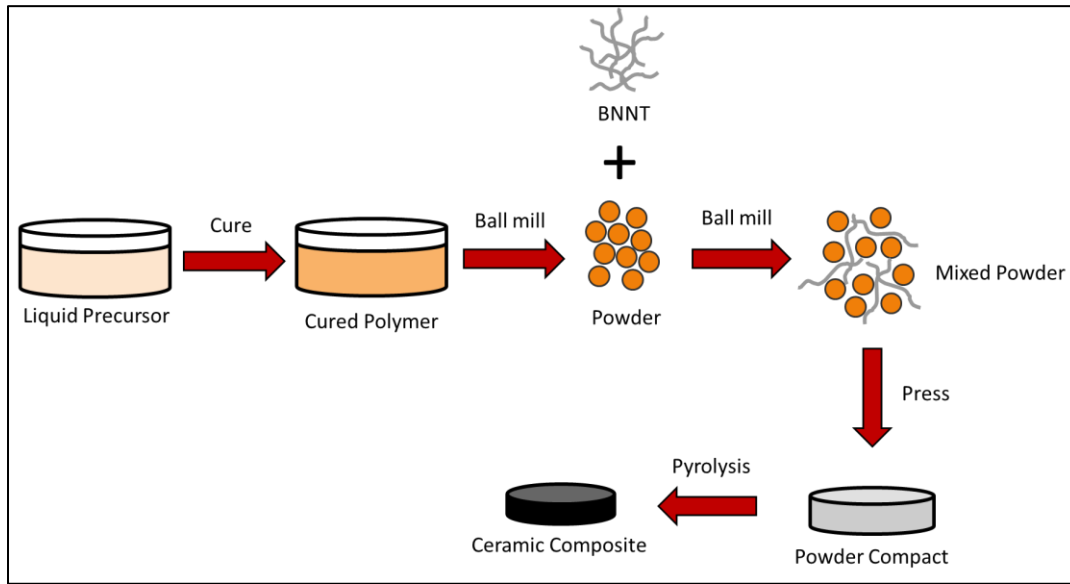


Figure 18. Schematic for ball-milling mixing method

3.3 Results

Firstly, the effect of BNNTs on the density and porosity of the composites were investigated. The density was calculated by measuring the weight and volume of the samples (ρ_{measured}). The theoretical density of fully dense SiCN is 2.4 g/cm³ (KiON data sheet) and the theoretical density of BNNTs is 1.38 g/cm³ [89]. The theoretical density of the composite ($\rho_{\text{theoretical}}$) can be calculated using the following formula:

$$\rho_{\text{theoretical}} = \rho_{\text{SiCN}} \times V_{\text{SiCN}} + \rho_{\text{BNNT}} \times V_{\text{BNNT}}$$

where ρ is the theoretical density and V is the volume fraction of the material. The volume fraction of BNNT (V_{BNNT}) within the composite can be calculated with weight percentages using the following formula:

$$V_{BNNT} = \frac{\frac{W_{BNNT}}{\rho_{BNNT}}}{\frac{W_{BNNT}}{\rho_{BNNT}} + \frac{W_{SiCN}}{\rho_{SiCN}}}$$

where W is the weight percent. The porosity (P) of the composite can then be calculated using the following formula:

$$P = \left(1 - \frac{\rho_{measured}}{\rho_{theoretical}}\right)$$

Table 4 shows multiple measurements for the samples, including the measured density and porosity. The BNNT composites had less porosity and higher density than the pristine sample (0 wt%). The porosity decreased and the density increased as the weight percentage of BNNT increased. The only sample that did follow the density increasing trend was the 20 wt% sample which was slightly less dense than the 10 and 15 wt% samples but still more dense than the pristine sample. It is not entirely clear why this occurred with 20 wt% sample. Perhaps insufficient pressure was applied during the powder pressing phase that caused this decrease in density. Unfortunately, I was unable to make another 20 wt% sample to test this density measurement anomaly due to the expensive cost of BNNT. Another trend that was discovered was a decrease in shrinkage along the diameter of the samples when the BNNT weight percentage was increased. Similarly, the weight lost after pyrolysis decreased when the BNNT weight percentage increased. Although the composites were slightly larger in volume compared to the pristine sample, the composites retained much more weight which caused the density increase. This densification and decrease in diameter shrinkage are due to BNNT acting as an inert filler. As previously mentioned in the literature

review, one of the major drawbacks of PDCs is the major shrinkage (~20%) that occurs during the thermal treatment transformation process.

Table 4. Ball-milling mixing sample measurements

Sample	Diameter (mm)	Thickness (mm)	Weight Loss after pyrolysis (%)	Measured Density (g/cm³)	BNNT Volume fraction (%)	Porosity (%)
Control	11.41	1.564	31.9	1.28	0	46.7
5 wt%	12.09	1.275	21.3	1.45	8.39	37.3
10 wt%	12.2	1.525	18.1	1.61	16.19	28.0
15 wt%	12.35	1.366	11.5	1.62	23.48	25.0
20 wt%	12.42	1.461	7.3	1.57	30.30	24.9
25 wt%	12.76	1.336	4.4	1.68	36.70	17.1

The microstructure of the composites was investigated using SEM analysis. The surface of the pristine and 5 wt% sample can be seen in Figure 19. The pristine sample shows the amorphous ceramic sections (of various sizes) being separated by loose boundaries and many pores are present. While the 5 wt% sample showed more dense ceramic sections with tighter boundaries and fewer pores. With only a 5 wt% addition of BNNT one can see a significant increase in density and decrease in porosity in the microstructure of the composite. These results were similar for the other composites and correlate with the measured values of the density and porosity. The cross-sections of the samples were also investigated with SEM (Figure 20). The cross-sections were exposed by fracturing the samples while being submerged in liquid nitrogen to maintain a smooth fracture. The SEM images of the cross-sections showed a similar trend to the surface microstructure. The control sample had more porosity and was less dense when compared to the composites. These SEM results further reinforce the densification effect BNNTs have on the

ceramic matrix. SEM was also used to examine BNNT dispersion. However, during my investigation it was very difficult to locate the nanotubes, which could imply poor BNNT dispersion from my mixing method. The only nanotubes found were either bent or twisted (Figure 21). I believe these nanotubes might have been damaged by the aggressive nature of the ball-milling mixing process.

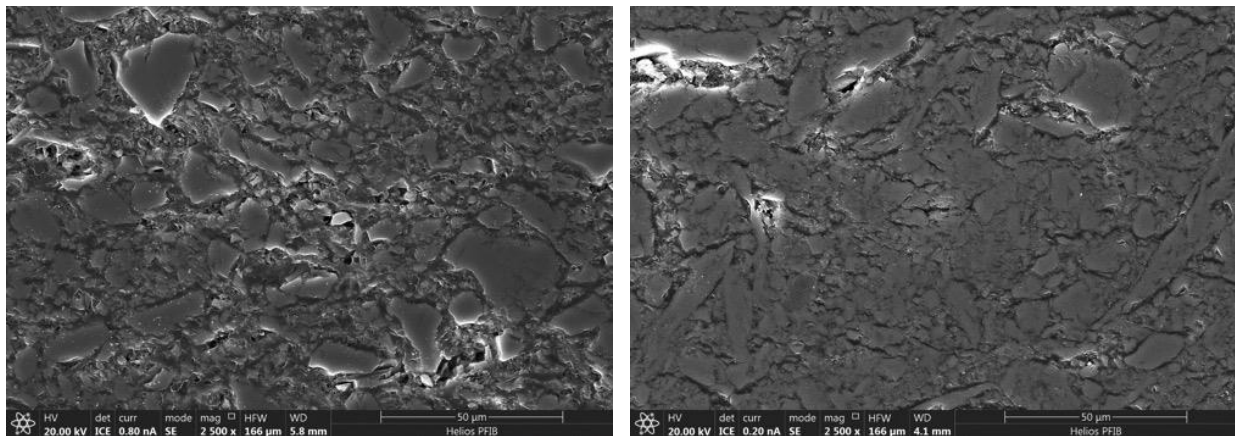


Figure 19. SEM surface view: control sample (left) and 5 wt% sample (right)

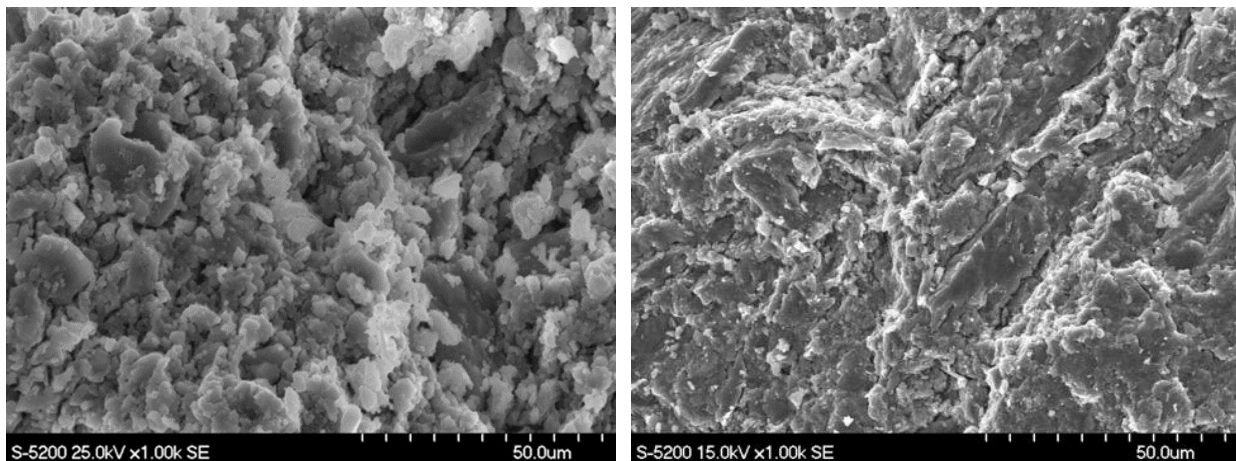


Figure 20. SEM cross section view: control (left) and 15 wt% (right)

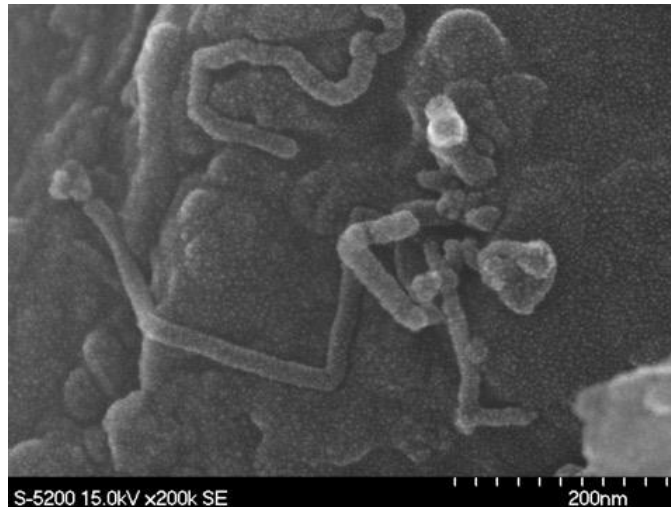


Figure 21. SEM cross section view: 'Damaged' nanotubes (15 wt%)

The mechanical properties of these samples were measured using the Vickers microhardness test. The samples were loaded into the Vickers hardness machine and were indented with a load of 500 gf. The diagonals of the diamond shaped indentation were measured using an optical microscope imaging software. These lengths were then used to calculate the Vickers hardness values which can be converted into MPa by multiplying by 9.807. The hardness results can be seen in Table 5. The hardness increased as the BNNT weight percentage increased, the only exception, again, was the 20 wt% sample which did not follow this trend. The 20 wt% sample had slightly less hardness than the 10 and 15 wt% sample, which is identical to the density results for these samples. Density plays a major role in a material's hardness, as visualized in Figure 22, which shows both the density and hardness results having identical trends. The composite samples have less porosity and a higher concentration of ceramic sections which allows them to resist more deformation. It is important to note the hardness of 25 wt% sample was not tested because it was required for a different experiment. However, it was expected to have the highest hardness because it had the highest density of all the samples.

Table 5. Vickers Hardness Results

Sample	Vickers Hardness	Hardness (GPa)	Density (g/cm ³)
Control	170.6	1.67	1.28
5 wt%	289.4	2.84	1.45
10 wt%	347.5	3.41	1.61
15 wt%	355.5	3.49	1.62
20 wt%	306.4	3.00	1.57
25 wt%	-	-	1.68

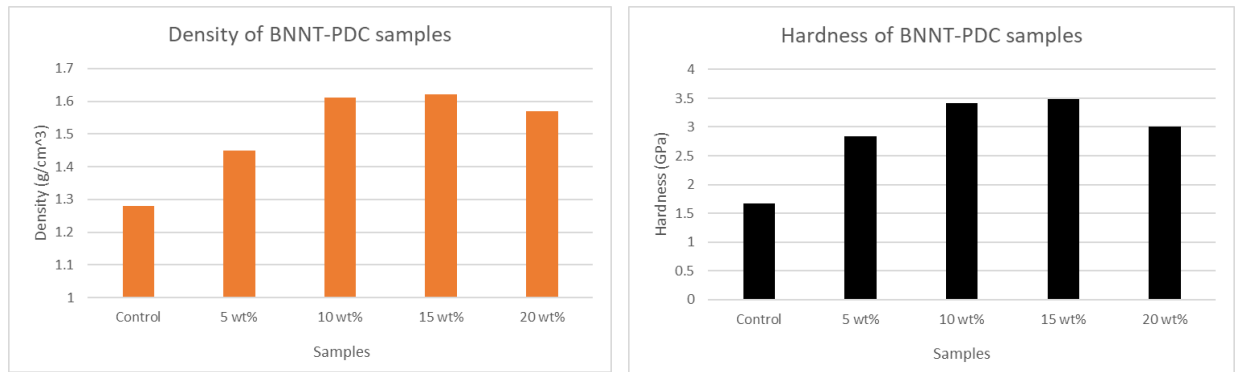


Figure 22. Density and Hardness of BNNT-PDC

3.4 Summary

This was the first method used to successfully create BNNT-SiCN composites during my research. This method allowed us to create composites with high BNNT weight percentages (up to 25 wt%) which is not common in BNNT composites from previously published work. The BNNT in the composites acted as an inert filler which slightly reduce ceramic shrinkage and greatly reduced weight loss during pyrolysis. This resulted in the composites becoming denser (and less porous) as the BNNT content increased. The 25 wt% sample was 31% more dense and

30% less porous than the pristine ceramic. The microstructure was investigated with SEM and further proved the densification effect of BNNT on the ceramic. The composites had less porosity and tighter ceramic granules which helped increase the material's hardness. The 15 wt% sample had the highest recorded hardness at 3.49 GPa which was 200% harder than the pristine sample. However, I believe the ball-milling mixing method was too aggressive for the BNNT and potentially damaged the nanotubes. I also believe ball-milling was not effective at dispersing the BNNTs in the ceramic matrix because it was very difficult to locate the nanotubes under SEM.

Chapter 4: Polymer Infiltration and Pyrolysis (PIP) Method

4.1 Introduction

Another method used to create fully dense ceramic matrix composites involves infiltrating the reinforcing material (usually fibers) with the liquid polymer precursor. This infiltration process is typically vacuum-assisted which helps the precursor fill up the space between the fibers to create a more compact matrix. This process is known as the polymer infiltration and pyrolysis (PIP) method and it offers significant manufacturing flexibility compared to other CMC fabrication processes [24]. However, even with a fully infiltrated matrix, porosity will be formed during pyrolysis because of the formation of gases during the ceramic transformation. The porosity can be reduced by repeating the polymer infiltration and pyrolysis process many times. This re-infiltration significantly reduces porosity and increase the overall hardness of the matrix.

The PIP method was used to make the first set of thin BNNT-SiCN composites. The first step is to create BNNT mats which were manufactured in the lab by filtrating a BNNT solution with a Teflon filter paper. The BNNT mats had an average thickness of $\sim 30 \mu\text{m}$ and density of $\sim 0.7 \text{ g/cm}^3$. The mats were slightly flexible but not very tough because they could be torn easily. The mat was cut into the desired shape and then the liquid precursor was infiltrated. Once the BNNT mat was full soaked with the polymer precursor, it underwent pyrolysis to create the ceramic composites. These composites had a BNNT weight percentage of about 35%.

This method was heavily inspired by this lab's previous work on applying the PIP method to create CNT-SiCN composites [90]. An aligned carbon nanotube sheet was infiltrated with Polysilazane (PSZ) to create strong and ultra-flexible ceramic composites. Figure 23 shows the samples during different steps of the PIP process. Although the CNT was fully infiltrated with the precursor (Figure 23.b), porosity is formed in the ceramic matrix after the 1st cycle of PIP (SiCN1)

because of the gases formed during pyrolysis (Figure 23.c). A 2nd cycle of PIP (SiCN2) can be used to reduce porosity (Figure 23.d). The mechanical properties of these samples were measured and the results can be seen in Figure 24. The CNT/SiCN1 sample improved the tensile strength and Young's Modulus by 208% and 1108%, respectively, compared to the CNT sheet. The mechanical properties were slightly improved with a second cycle of PIP, with a 223% increase in tensile strength and 1289% increase in Young's Modulus when compared to the pristine CNT sheet.

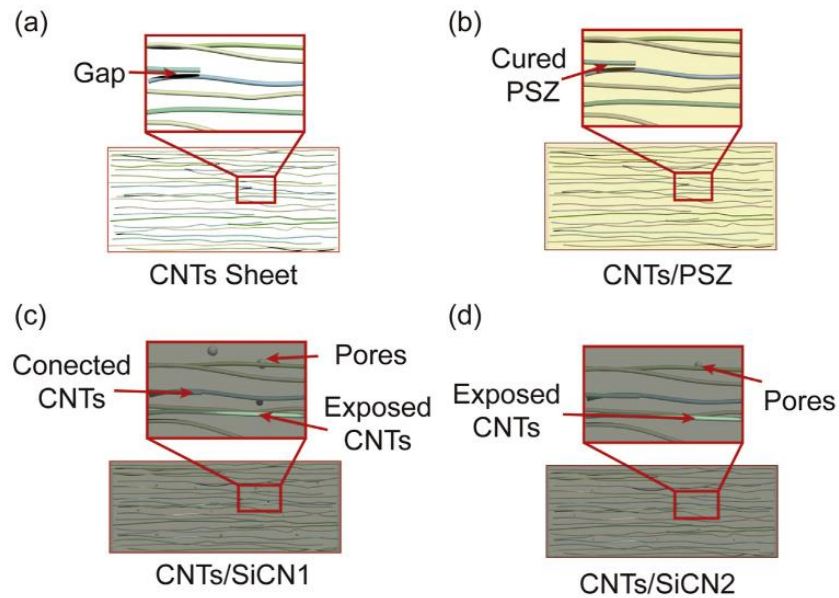


Figure 23. Illustration of PIP process to prepare CNT reinforced SiCN composites. a) CNT sheet, b) CNT/PSZ, c) CNT/SiCN1, and d) CNT/SiCN2 [90]

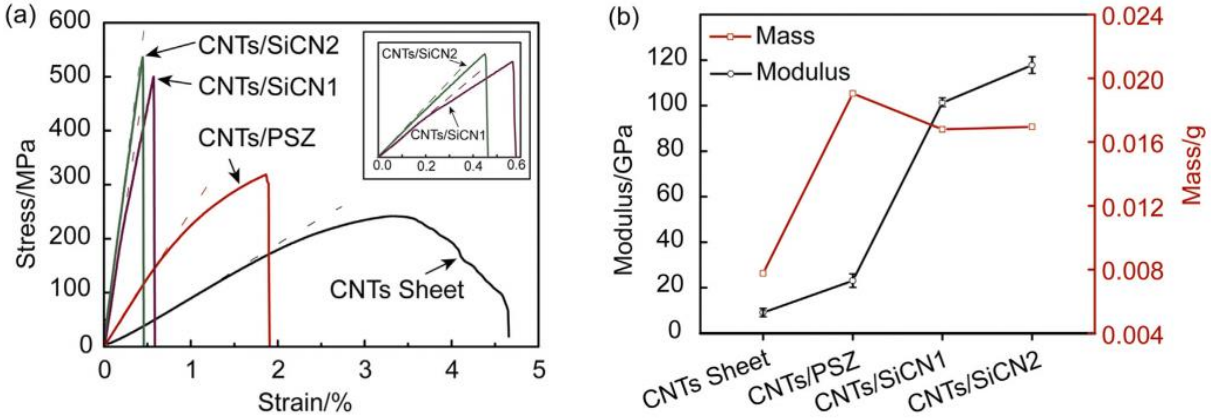


Figure 24. Mechanical properties of CNT-SiCN composites. a) Stress-strain curve and b) Young's Modulus [90]

4.2 Experimental

Figure 25 illustrates the steps used to make composites with the PIP method. The first step is to create a BNNT mat (thin sheet of BNNT). BNNT puffball (from BNNT, LLC, Newport News, VA), CTAB (surfactant) and water were mixed to disperse the BNNT in a liquid solution. The BNNT solution was created using the following ratio: 100 mg of BNNT, 100 mg of CTAB and 40 ml of water. This ratio was recommended and used by NASA Langley Research Center to make BNNT solutions. The solution is then mixed and mechanically stirred at 600 RPM for about 4 days. Once the BNNT is fully dispersed, the solution is filtered using vacuum filtration. Hydrophilic Teflon filters with a pore size of 0.2 μm were used to filter the water from the BNNT solution. Once all the water has been filtered out, a circular BNNT mat is deposited on the Teflon filter. The BNNT mat is carefully removed from the filter to prevent tearing or damaging the mat. The mat was then cut into rectangular shapes ($L = 23 \text{ mm}$ and $W = 5.2 \text{ mm}$) using a razor blade. The cut mats had a density of about 0.68 g/cm^3 and a porosity of about 51%.

Polysilazane (PSZ, KiON Defense Technologies, Inc., Huntingdon Valley, PA) was mixed with 4 wt% dicumyl peroxide (thermal initiator). The mats were infiltrated with the precursor by

submersing them in the precursor and applying vacuum. Vacuum was applied for 15 minutes and during this process bubbles formed (Figure 26), caused by the removal of air within the mat. Once fully infiltrated, the mats were manually pressed between paper towels to remove all excess precursor on the surface of the mat. This step is important to prevent a thin layer of SiCN from forming on the surface. The soaked mats were then placed in the tube furnace to cure at 140 °C for 16 hours in air atmosphere. The samples then underwent pyrolysis in the tube furnace at 1000 °C for 1 hour in a nitrogen atmosphere with a ramp up rate of 1 °C/min and a ramp down rate of 2 °C/min. A glass quartz (Figure 27) was placed on top of the mat during both curing and pyrolysis to help maintain a flat shape.

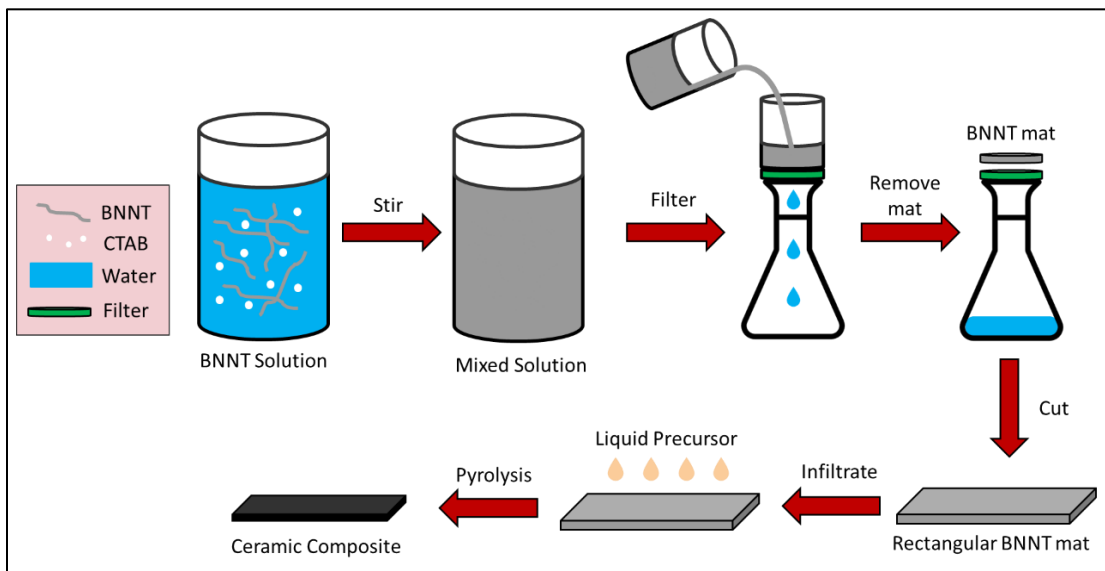


Figure 25. Schematic for PIP method



Figure 26. BNNT mats submersed in precursor and exposed to vacuum



Figure 27. Quartz glass placed on top of composite mat to help prevent warping during heat treatment

It is important to note, the method described above is the optimized PIP manufacturing method. The first set of samples made with the PIP method were not very successful. The samples had either cracked or warped during pyrolysis (Figure 28). This was most likely caused by an uneven distribution of liquid precursor within the BNNT mat. Initially, the mats were infiltrated with liquid PSZ via pipet droplets with vacuum being applied on the bottom side of the mat. Once the mats were fully soaked with liquid precursor on the top side, they were flipped over to infiltrate the opposite side. If one side of the BNNT mat had more precursor, then during pyrolysis this side would shrink more which could explain why the samples were either bent or broken. The manufacturing process was optimized by using the submersion vacuum technique, removing excess precursor with the paper towel, and placing the glass quartz on the sample during heat treatment. Figure 29 shows a crack-free and flat BNNT-SiCN sample created from the optimized manufacturing method.



Figure 28. Side view of BNNT-SiCN sample (28 wt%) with initial manufacturing method



Figure 29. Top view of BNNT-SiCN sample (35 wt%) with improved manufacturing method

4.3 Results

The dimensions of the BNNT mat and composite were measured to calculate density. The theoretical density of BNNT is 1.38 g/cm^3 and fully dense SiCN is 2.4 g/cm^3 . The porosity of the samples was calculated with the porosity formula (Chapter 3.3). The BNNT mat had a measured density of 0.72 g/cm^3 and a porosity of 47.8%. With the PIP process, the BNNT-SiCN composite was able to increase density by 218% and decrease porosity by 30.2%. A third sample was made by film-casting the precursor to create a thin film of SiCN. This pristine ceramic sample had a density of 2.03 g/cm^3 and a porosity of 15.4%. All these measurements can be seen in Table 6. It is important to note, multiple composites were created with the PIP method. Most composites had similar densities, BNNT weight percentages, and porosities. Therefore, this method does not allow the composite BNNT weight percentage to be fully controlled.

Table 6. PIP sample measurements

Sample	BNNT weight percentage (%)	Measured Density (g/cm^3)	BNNT Volume fraction (%)	Porosity (%)
BNNT Mat	100	0.72	100	47.8
BNNT-SiCN	35	1.57	48.4	17.6
SiCN Film	0	2.03	0	15.4

The microstructure of these samples was investigated using SEM. Figure 30 shows the pristine BNNT mat and amorphous SiCN SEM images. The BNNT mat consisted of many BNNTs (as well as some impurities) entangled in a random nature with large amounts of empty space between the tubes, which explains the high porosity. On the other hand, the SiCN film had a fully dense amorphous matrix with a few microcracks. Figure 31 shows SEM images of the cross-sectional view of the BNNT-SiCN sample. The cross sections were exposed by submersing and breaking the samples in liquid nitrogen to ensure a smooth fracture. The cross section shows a high concentration of BNNTs within the ceramic matrix and some BNNT pullout, which could imply some improvements in toughness for the composite. Figure 32 shows SEM images of the surface of the surface of the BNNT-SiCN. In general, the SiCN was able fill up the matrix and remove most empty spaces between the nanotubes. A second cycle of PIP could have helped reduce this porosity, but it was not pursued after the mechanical test results after the 1st cycle of PIP.

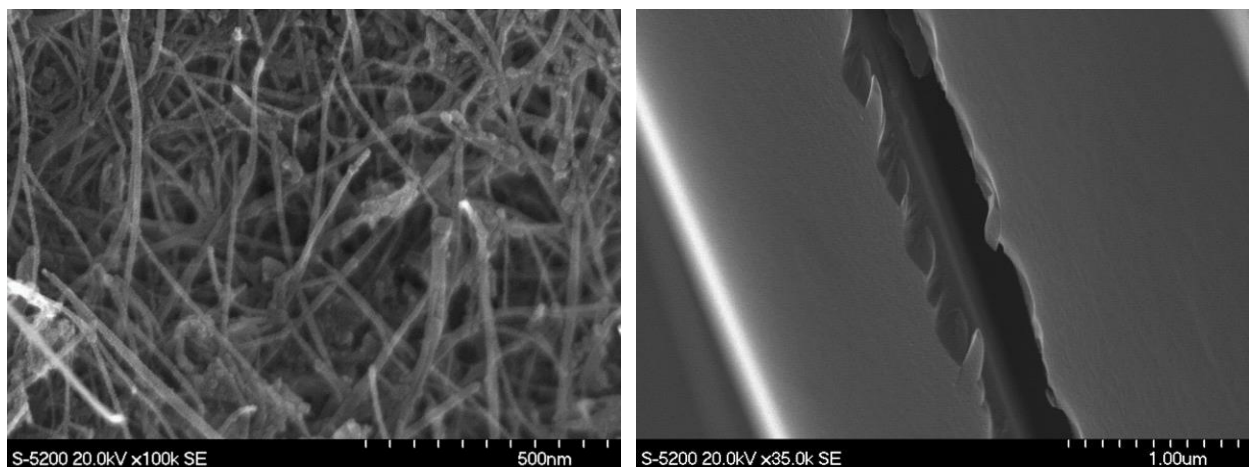


Figure 30. SEM surface view of: BNNT mat (left) and SiCN film (right)

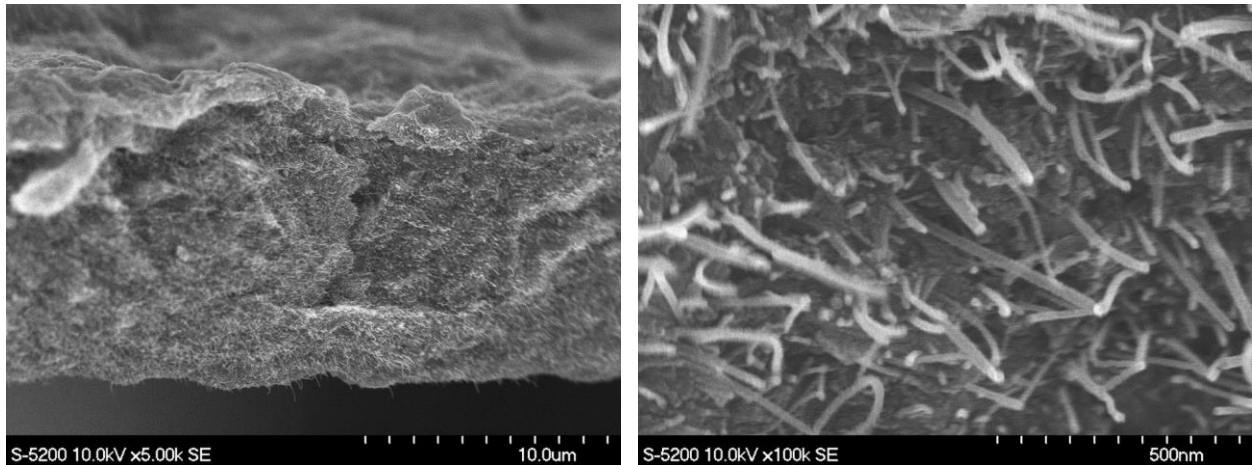


Figure 31. SEM cross section view of BNNT-SiCN (35 wt%)

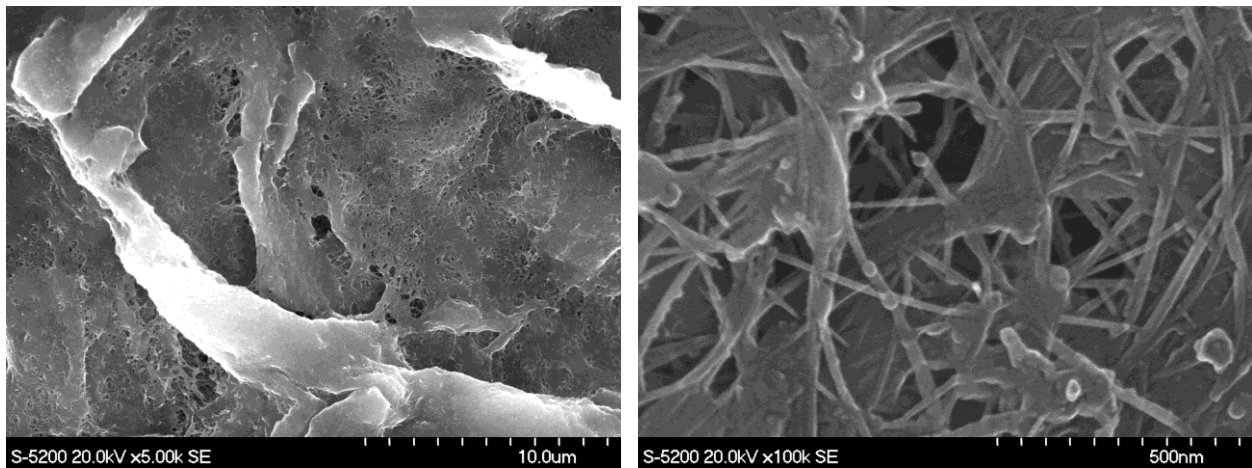


Figure 32. SEM surface view of BNNT-SiCN (35 wt%)

Since these samples were very thin (micron scale) Knoop Hardness was used instead of Vickers. The indentation for Knoop is smaller and recommended for samples with small cross-sectional areas. The samples were loaded on the micro-hardness machine and indented using a load of 50 gf. The diagonal was measured with an optical microscope imaging software and the Knoop hardness was calculated (Table 7). The unitless HV value can be converted into MPa by multiplying by 9.807. Unfortunately, the composite was not stronger than the pristine SiCN. The pristine sample was 347% harder than the composite. Therefore, there was no improvement of mechanical properties for the composite when compared to the pristine ceramic. However, from a

different perspective, the research shows the composite had better mechanical properties when compared to the BNNT mat. The composite had a hardness of 3.74 GPa which is 2330% higher than the hardness of the BNNT mat. It is important to note that the samples were embedded in epoxy for the micro-hardness test. So, there is a possibility the epoxy infiltrated the porous BNNT mat and affected the micro-hardness results. Epoxy has a Knoop hardness of around 20 which is about 0.2 GPa and a density of about 1.1 g/cm³ [91]. This means the Knoop hardness value for the BNNT mat could be the value for a BNNT-epoxy composite. Assuming the epoxy was able to fully infiltrate the mat, the epoxy composite would have a BNNT weight percentage of about 52.2% and a theoretical density of 1.23 g/cm³. Therefore, the ceramic composite was significantly harder than an assumed epoxy composite.

Table 7. Knoop Hardness Results

Sample	BNNT weight percentage (%)	Knoop Hardness	Hardness (GPa)	Density (g/cm³)
SiCN Film	0	1324	12.98	2.03
BNNT-SiCN	35	381.4	3.74	1.57
BNNT Mat (with epoxy)	52.2	16.1	0.16	1.23

4.4 Summary

This was the second method to successfully create BNNT-SiCN composites. The manufacturing process was optimized to create flat and crack-free composites. One drawback with this method is not being able to control the BNNT weight percentage in the composite. Most of the composites had about 35 wt% of BNNT. The composites increased density by 218% and decrease porosity by 30.2% when compared to the very porous BNNT mat. The polymer precursor

seemed to infiltrate and fill up most of the empty spaces between the nanotubes. The cross-section of the composite displayed some BNNT pull-out which implied the BNNT could be strengthening the ceramic matrix. However, after running the micro-hardness test, I discovered the composite was not stronger than the pristine ceramic material. The non-reinforced ceramic film was 347% harder than the composite. A second cycle of PIP could have been used to reduce some of the porosity of the composite, but it only would have increased the mechanical properties slightly. Therefore, the addition of BNNT did not improve the mechanical properties of the composite. I believe we can revisit this method once we have better BNNT mats with less impurities and more aligned tubes.

Chapter 5: Precursor Mixing Method

5.1 Introduction

After the results from the thin BNNT-SiCN composites (Chapter 4), I decided to return to manufacturing bulk composites. After the results from Chapter 3, a new technique to add the BNNT into the ceramic matrix was needed, one effective at dispersing the BNNTs but that would not harm the nanotubes. I was curious to see if I could take advantage of the liquid precursor phase and disperse the BNNT directly in the precursor. To my surprise, the BNNTs dispersed in the liquid precursor with only mechanical stirring and no surfactants were needed.

The precursor mixing method was used to create the second set of bulk BNNT-SiCN composites. The BNNTs are added to the liquid precursor and mixed using a magnetic stirrer. The solution was stirred until the BNNTs were fully dispersed, which took about 4 days. The homogenous solution was then poured into a mold to cure. The cured composite was then removed from the mold and underwent pyrolysis to form the ceramic matrix. With this method only composites with small weight percentages can be made (up to 0.5 wt%), as adding too much BNNT in the liquid precursor will make the solution too viscous, causing poor BNNT dispersion.

5.2 Experimental

Figure 33 illustrates the steps used to make BNNT-SiCN composites with the precursor mixing method. Polysilazane (PSZ, KiON Defense Technologies, Inc., Huntingdon Valley, PA) was mixed with 2 wt% dicumyl peroxide (thermal initiator). Raw puffball BNNT (from BNNT, LLC, Newport News, VA) was added to the liquid precursor and mechanically stirred (>1000 RPM) for 3 days. On day 3, most of the BNNT was dispersed in the precursor but a few clusters of BNNTs were still present (Figure 34). The mixture was then placed in a sonication bath for 5 minutes, to help break up the clusters. It was then stirred for 1 more day and on the 4th day the

BNNT was fully dispersed in the precursor (Figure 34). The solution was then poured into different molds (Figure 35) and cured at 140 °C for 16 hours in an air atmosphere. The cured samples were then removed from the molds and underwent pyrolysis at 1000 °C for 1 hour in a nitrogen atmosphere with a ramp rate up and down rate of 1 °C/min. Only composites with 0.1 and 0.5 wt% of BNNT were feasible with this method.

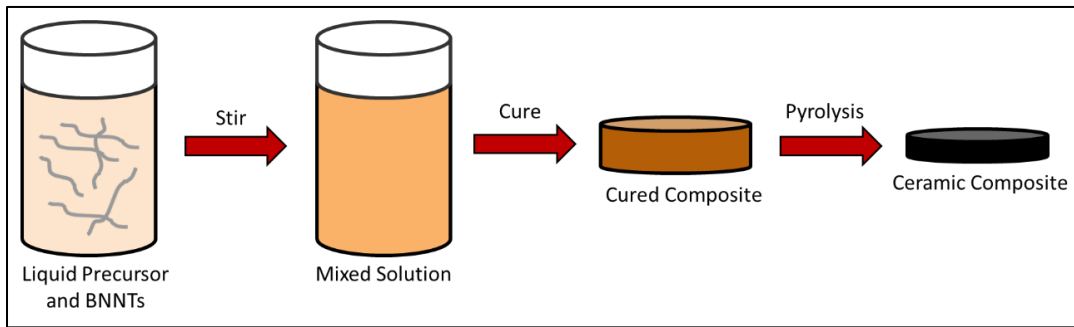


Figure 33. Schematic for precursor mixing method

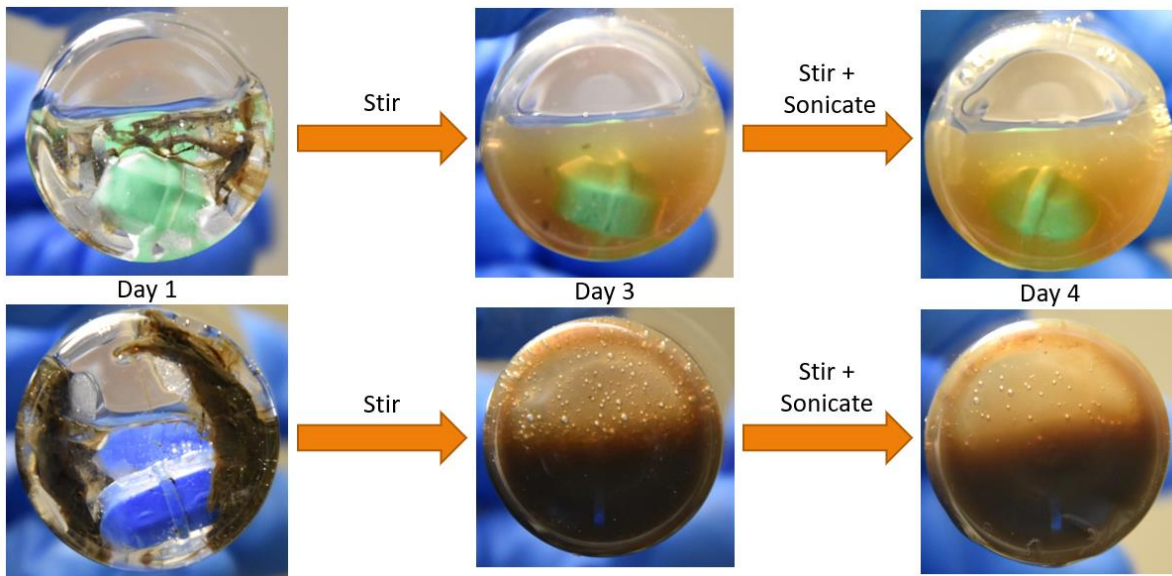


Figure 34. BNNT-PSZ solution time lapse: 0.1 wt% (top row) and 0.5 wt% (bottom row)



Figure 35. Rubber Mold (left) and Teflon beaker (right) [ruler units = cm]

5.3 Results

This method allowed us to create samples with different shapes by pouring the mixed liquid precursor solutions in molds before curing. The molds used for this research were a Teflon beaker and rubber mold. Figure 36 shows the cured samples before and after they were removed from the molds. A few of the samples were broken after curing, these fractures mainly occurred during the removal process. Removing the samples from the molds was somewhat difficult, especially from the rubber mold. A releasing agent should be used in the future to prevent the cured samples from sticking to the molds. From visual inspection, one can see the control sample (0 wt%) had less bubbles (porosity) than the composites after curing. These bubbles are the gases formed during the curing process that remained trapped in the matrix. The composite precursors were more viscous than the pristine precursor, which could explain why the gases had more difficulty being removed from the composites. Perhaps applying vacuum during curing could help reduce porosity for future samples. The cured circular 0.1 wt% sample showed the BNNT separating from the center of the sample and collecting around the edges (Figure 36). The cured precursor around the edges of the 0.1 and 0.5 wt% samples in the rubber mold also showed the BNNT conglomerating (Figure 36). This implies the precursor can only maintain the BNNT dispersion if mixing is applied. If no mixing is applied, the BNNT will separate from the liquid precursor. Figure 37 shows the sample before and after pyrolysis.

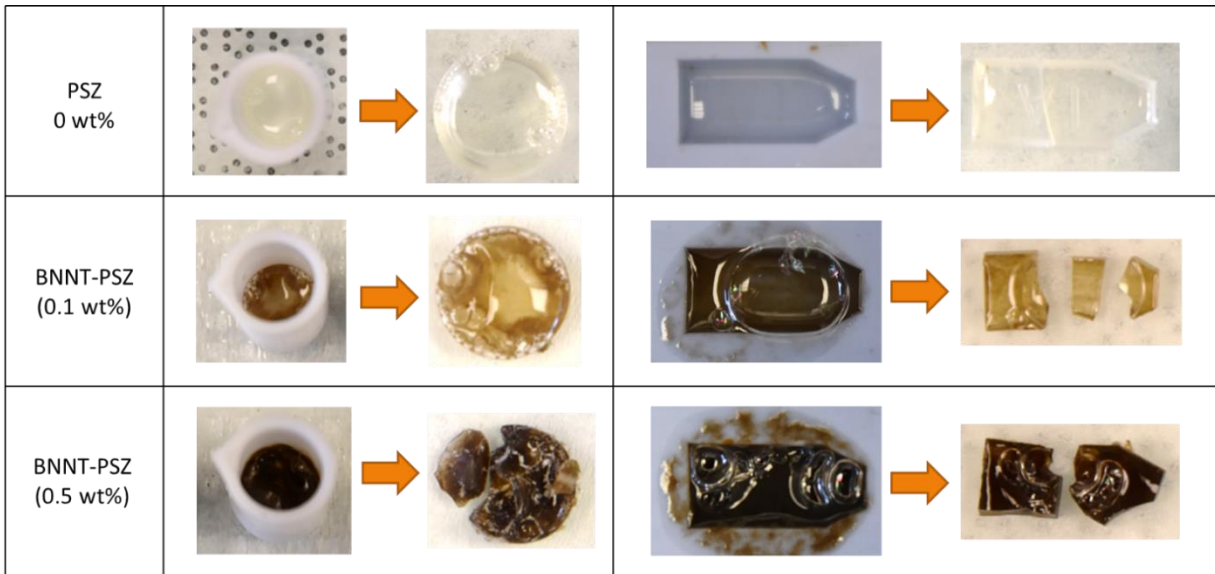


Figure 36. Cured precursor mixing samples removed from molds

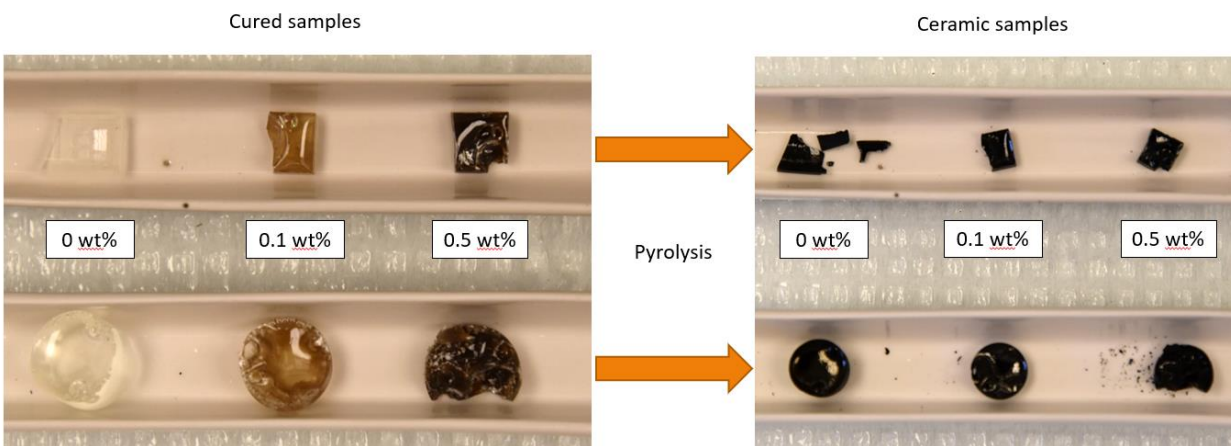


Figure 37. BNNT-SiCN before and after pyrolysis

The microstructure of these samples was investigated using SEM. The control sample's microstructure was fully dense with a few micro-cracks and nearly identical to the SEM image of the SiCN film seen in Figure 30 (Chapter 4). Figures 38 & 39 show the surface of both the 0.1 and 0.5 wt% samples. Both composite samples were fully dense with amorphous SiCN with little to no pores present. The BNNTs were somewhat scattered across the ceramic matrix and tended to cluster together in certain areas. A few of the BNNTs were entangled together to form an almost

rope-like structures. This could have been caused by the precursor not fully separating the BNNTs during the mixing phase or from the BNNTs separating from the precursor and clustering during the curing phase. A few micro-cracks were present in the composites, and certain locations showed the nanotubes extending from the cross-section of the cracked site (Figures 38 & 39). This display of BNNT pullout could suggest the BNNTs are improving the mechanical toughness of the composite.

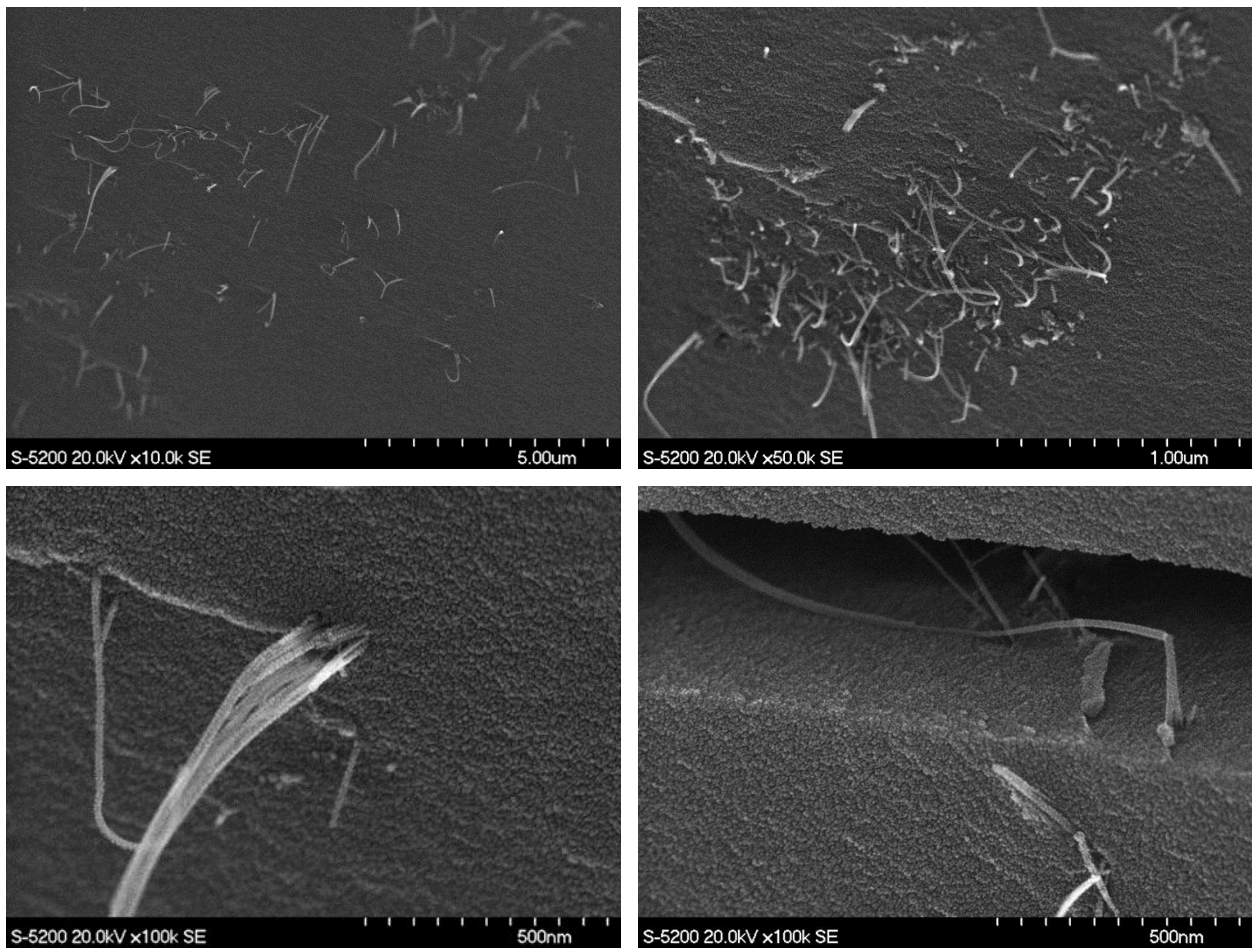


Figure 38. SEM surface view of BNNT-SiCN (0.1 wt%)

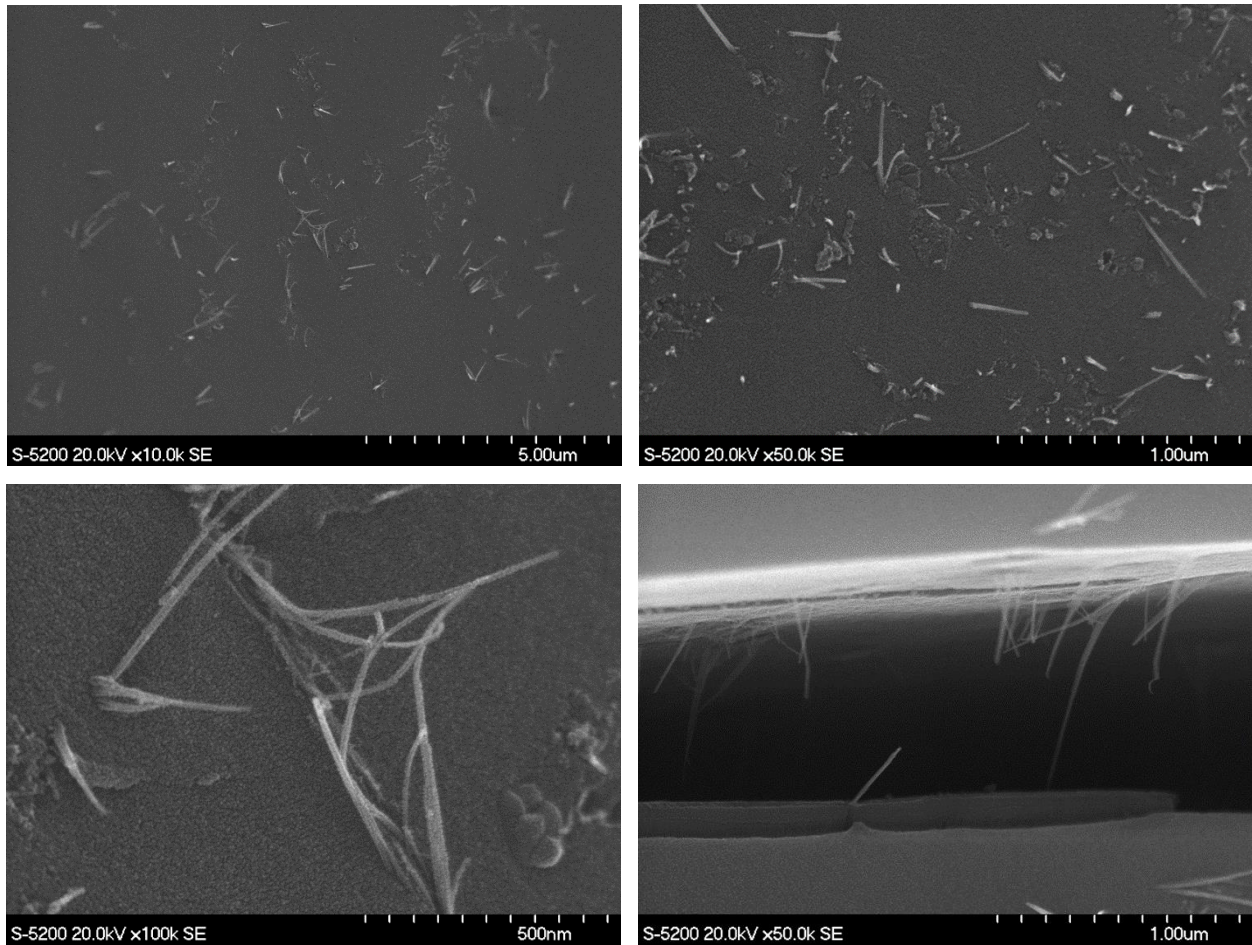


Figure 39. SEM surface view of BNNT-SiCN (0.5 wt%)

The microhardness of these samples was calculated using Vickers Hardness. The samples were placed in the micro-hardness machine and indented with a load of 500 gf. The diagonals were measured using an optical microscope imaging software to calculate the Vickers Hardness values (Table 8). The control sample had a hardness of 15.5 GPa, similar to fully dense SiCN hardness values from literature [8,23]. The composites had a slightly higher hardness than the pristine sample, with the 0.5 wt% having a 5.8% higher hardness than the control. This slight increase in hardness was expected due to the small amount of BNNT weight percentage added to the composites. Higher weight percentages need to be tested to see if the hardness scales up with increasing BNNT weight percentage.

Table 8. Vickers Hardness results

Sample	Vickers Hardness	Hardness (GPa)
0 wt%	1585	15.5
0.1 wt%	1649	16.2
0.5 wt%	1668	16.4

5.4 Summary

This was the third method to successfully create BNNT-SiCN composites. It involved taking advantage of the liquid precursor phase and dispersing BNNT directly in the polymer without any surfactants. One major drawback with this method is very small weight percentages of BNNTs can be added to the composites (0.1 and 0.5 wt%). If too much BNNT was added into the precursor, the precursor would become too viscous and the BNNTs would not fully disperse. During the curing phase, the composites had more porosity than the pristine polymer and the BNNTs began to separate from the precursor if no mixing was applied. The SEM images showed the BNNTs scattered and clustered in certain areas of the ceramic matrix. The 0.5 wt% composite had a hardness value 5.8% higher than the pristine ceramic. This slight increase was expected based on the small amount of BNNT added to the composite. This method could be improved by using a compatible surfactant to help improve BNNT dispersion and increase BNNT weight percentages.

Chapter 6: Ethanol Mixing Method

6.1 Introduction

The ball-milling mixing method (Chapter 3) had a few drawbacks, such as poor BNNT dispersion and an aggressive mixing method that could damage the nanotubes, but it did show promising mechanical improvements. I decided to return to this powder pressing route to discover a better technique to mix the BNNTs and the ceramic powders. A few BNNT ceramic composites have been created using ethanol to disperse ceramic powders (such as silicon nitride and alumina oxide) and BNNTs wrapped by PVP polymer [86]. This inspired me to experiment with ethanol and use it as the liquid medium to mix the preceramic powder and BNNTs.

The ethanol mixing method was used to create the third and final set of bulk BNNT-SiCN composites. The first step is to create the cured precursor powder (similar to Chapter 3) and the BNNT solution (similar to Chapter 4). The powder and BNNT solution are then dispersed in ethanol and mixed using a sonication bath. The mixed solution is left open overnight to evaporate the ethanol. The dried powder mixture is then collected, pressed and pyrolyzed (similar to Chapter 3) to create the final ceramic composite material. This method allowed us to create ceramic composites with different weight percentages of BNNT (0, 1, 5, 10, 20 wt%). The samples had an average diameter of about 12 mm and average thickness of about 3 mm.

6.2 Experimental

Figure 40 illustrates the steps used to make the BNNT-SiCN composites with the ethanol mixing method. Polysilazane (HTT-1800, from Extreme Environment Materials Solutions (EEMS), LLC) was mixed with 0.5 wt% of the proprietary liquid catalyst (CLC-PB058, from EEMS) and mixed for 30 minutes. The precursor was then placed in a crucible and cured at 150 °C for 3 hours in an air atmosphere. The cured product was then ball milled for 30 minutes to form

fine powder ($\sim 5 \mu\text{m}$). BNNT puffball (from BNNT, LLC, Newport News, VA), CTAB (surfactant) and water were mixed to make a BNNT solution with the following ratio: 100 mg of BNNT, 100 mg of CTAB and 40 ml of water. This ratio was recommended and used by NASA Langley Research Center to make BNNT solutions. The solution was then mixed and mechanically stirred at 600 RPM for about 4 days.

The preceramic powder and BNNT solution were then dispersed in ethanol. The preceramic powder was dispersed in the ethanol first (Figure 41.a) and then the BNNT solution was added to the mixture (Figure 41.b). The mixed solution was placed in a sonication bath for 5 minutes to ensure a good dispersion. The homogenous solution was then placed in the fume hood overnight to allow the ethanol to evaporate. The powder mixture dried up in small clumps of powder (Figure 42) and was collected. The pestle and mortar were used to break up these powder clumps back into the fine particle size. Before the powders were pressed, 2-3 drops of the liquid precursor were added and mixed with the pestle and mortar. The liquid precursor helps bind the powder together during the cold press. 0.5 grams of the powder was loaded into a circular die with a diameter of 14.85 mm. The powder was pressed at about 40 MPa and held at that pressure for 10 minutes. The compacts (Figure 43) then underwent pyrolysis at 1000°C for 3 hours in an argon atmosphere with a ramp up and down rate of $1^{\circ}\text{C}/\text{min}$.

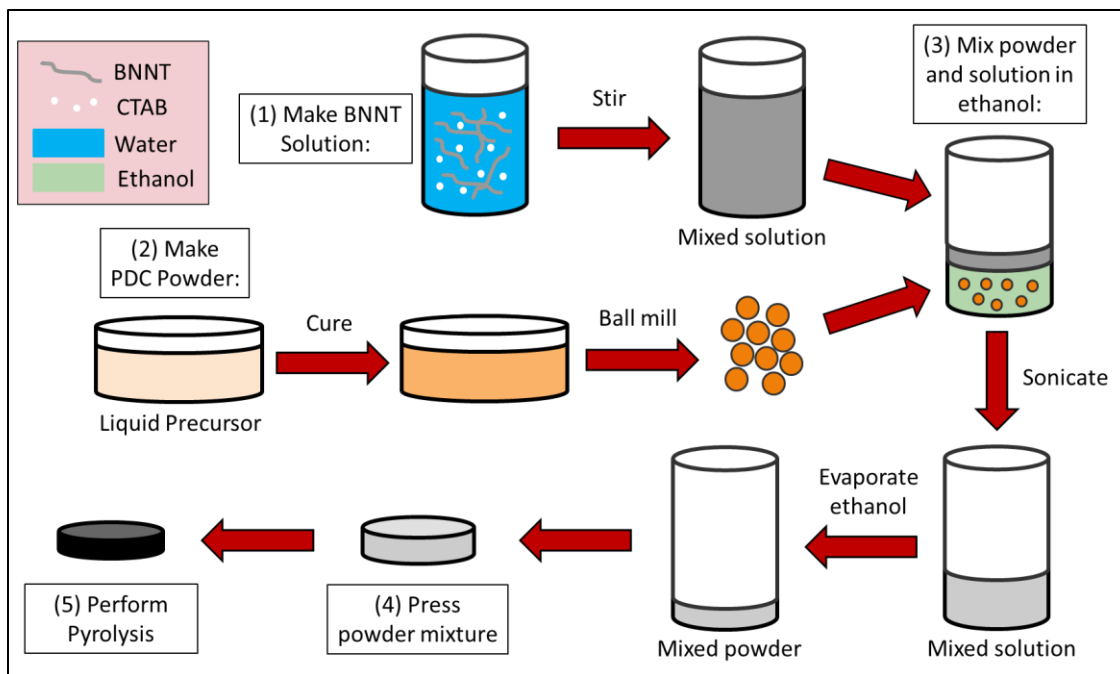


Figure 40. Schematic for ethanol mixing method

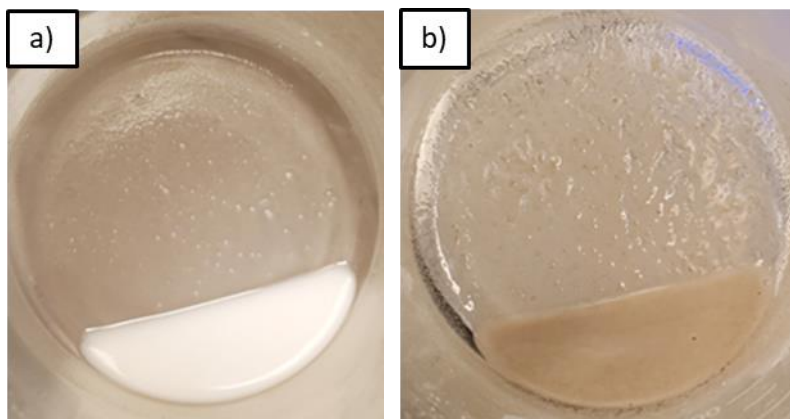


Figure 41. a) Ethanol mixed with preceramic powder and b) mixture with BNNT solution

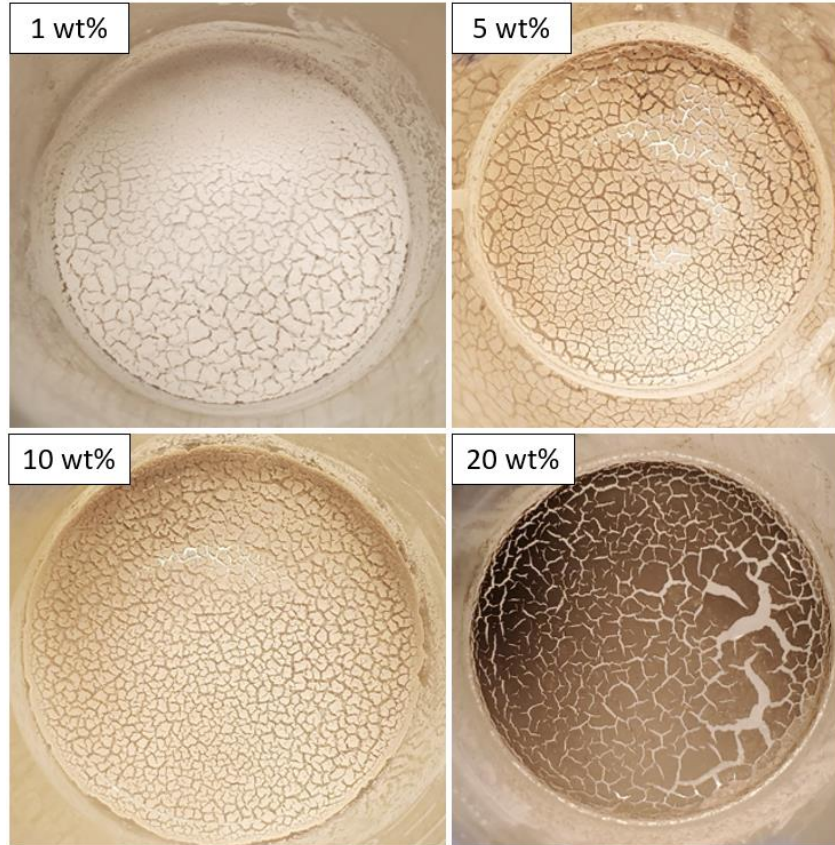


Figure 42. Dried up powder mixture once ethanol has evaporated



Figure 43. Pressed powder samples (0, 1, 5, 10, 20 wt%, respectively) before pyrolysis

6.3 Results

The dimensions of the ceramic samples were measured to calculate the density. Table 9 shows the measurements of the samples made with the ethanol mixing method. The porosity was calculated using the porosity formula (Chapter 3). The BNNT composites had higher densities than the pristine ceramic. Surprisingly, the composite with the highest density was the 1 wt%

sample which was 27.9% more dense and 14.7% less porous than the control samples. This was not the case for the ball-milling mixing samples, where the 25 wt% sample had the highest density. Also, the ball-milling mixing method showed higher density and the lower porosity as BNNT content increased. With the ethanol mixing method samples, there seems to be no correlation with density or porosity when increasing the amount of BNNT in the samples. However, we can see the diameter of the composites shrinks less as we add more BNNT. This implies BNNT is acting as an inert filler, which helps reduce shrinkage and weight loss during pyrolysis. Therefore, we would expect a steady increase in density as the BNNT content is increased (similar to the Chapter 3 results). Perhaps the powder compacts were not pressed with enough pressure to remove all the excess porosity or the powder needed to be ball milled more to make a finer powder. The densification of these samples should be revisited in the future.

Table 9. Ethanol mixing method sample measurements

Sample	Diameter (mm)	Thickness (mm)	Weight Loss after pyrolysis (%)	Measured Density (g/cm³)	BNNT Volume fraction (%)	Porosity (%)
Control	11	3.1	28.0	1.22	0	49.2
1 wt%	11.3	2.8	12.4	1.56	1.73	34.5
5 wt%	11.9	3.0	13.9	1.29	8.39	44.3
10 wt%	11.9	2.9	12.1	1.36	16.19	39.1
20 wt%	12.2	2.8	14.0	1.31	30.30	37.3

The ethanol-mixed powder and the ball-milling-mixed powder (Chapter 3) were compared. A 1 wt% ball-milling mixed powder was recreated by adding BNNT puffball in the powder and ball-milling for 30 minutes. Figure 45 shows the 1 wt% mixed powder from both methods. The ball-milling mixed powder (Figure 45.a) was white (same color as the pristine powder) with tiny

dark grey spots scattered around the powder. These spots are most likely tiny clusters of BNNT. Which implies the ball-milling mixing was not effective at fully dispersing and breaking down the BNNT in the powder. On the other hand, the ethanol mixed powder (Figure 45.b) was beige with no visible BNNT clusters. The beige color suggests the ethanol was able to successfully disperse the dark grey BNNT and white powder. SEM images of both mixed powders were taken to further investigate the BNNT dispersion. Figure 46 shows two different locations of the 1 wt% ball-milling mixed powder. The first location shows little to no BNNTs while the second location shows a high density (cluster) of BNNTs around the powder particles. Figure 47 shows the 1 wt% ethanol mixed powder at two different locations. Both locations seem to have a somewhat even distribution of the nanotubes between the powder particles and no large BNNT clusters were located. This reinforces the theory that ethanol mixing is more effective at dispersing the BNNTs than ball-milling.

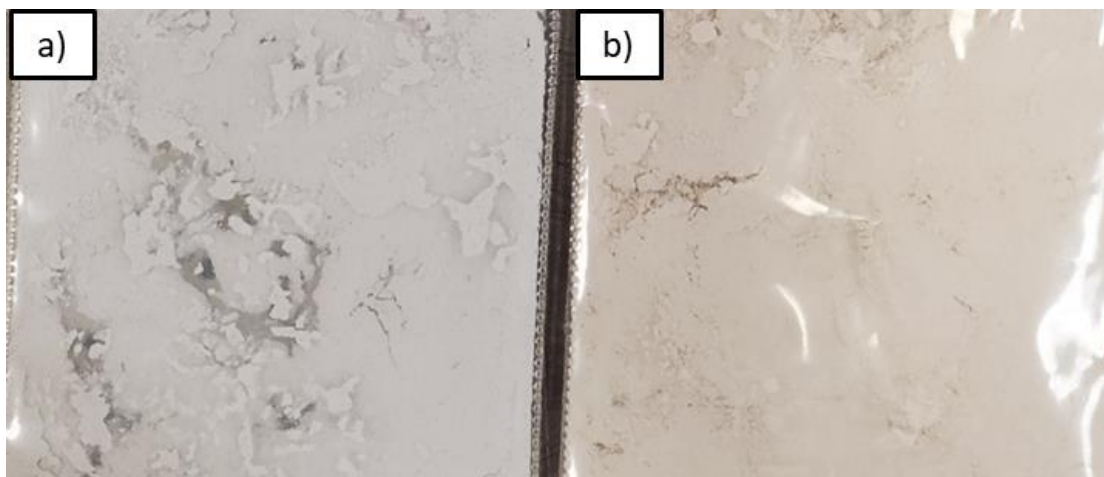


Figure 45. 1 wt% mixed powder: a) Ball-milling mixed powder and b) ethanol mixed powder

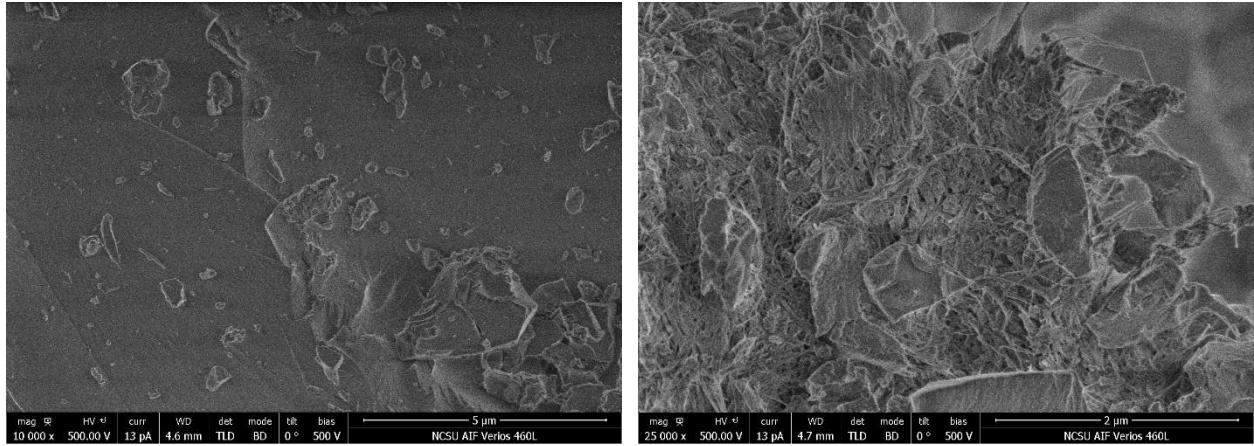


Figure 46. SEM image of 1 wt% ball-milling mixed powder

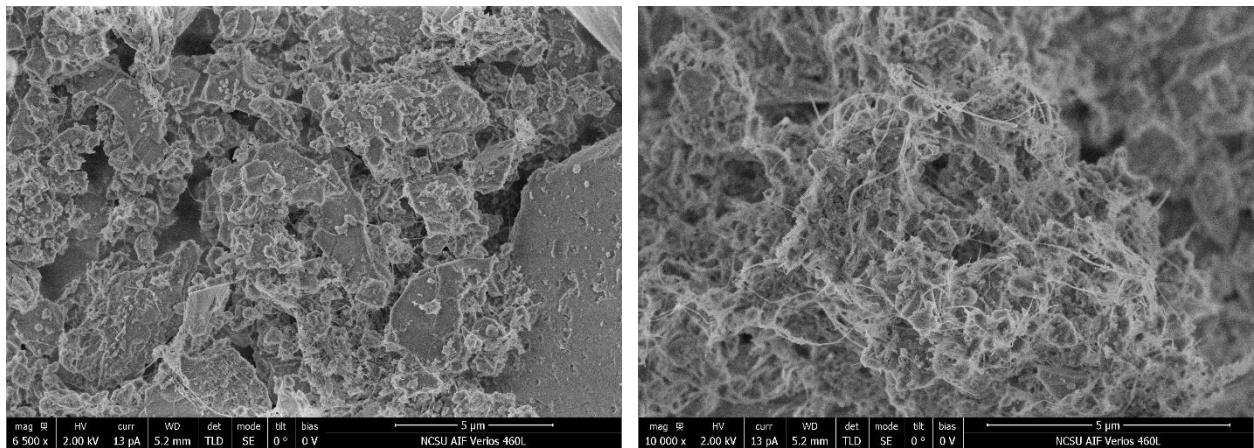


Figure 47. SEM image of 1 wt% ethanol mixed powder

The microstructure of the samples was also investigated with SEM. The cross section of the samples were exposed by using a razor blade to fracture the samples. The only sample that could not be broken with the razor blade was the 1 wt% sample, it was extremely tough and a larger shear was required to fracture this sample. Figure 48 shows the cross section of the pristine ceramic having large open areas between the amorphous SiCN sections, which was anticipated due to 49.2% calculated porosity. The cross section of the 1 wt% sample showed a much denser and flatter microstructure (Figure 49). Overall, the BNNTs were fairly scattered across the ceramic matrix but there were sections with high concentrations of nanotubes. Figure 50 shows the cross

section of the 5 wt% sample which had a good dispersion of BNNTs but was more porous than the 1 wt% sample. The reason is not clear why the 1 wt% sample was much denser than the other composites. Perhaps adding 1 wt% of BNNT is the optimal SiCN composites. More samples need to be created before this claim can be made.

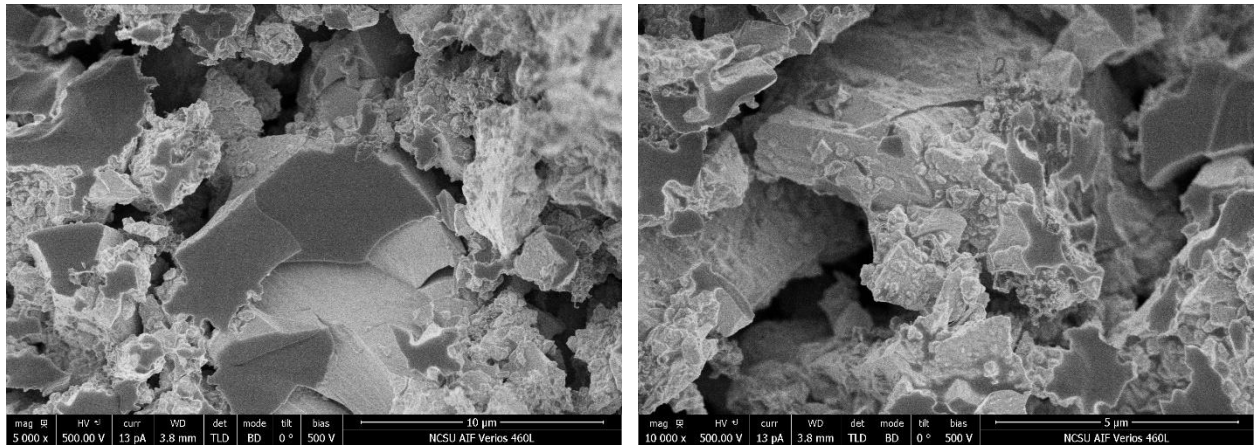


Figure 48. SEM cross section view of ceramic 0 wt% sample

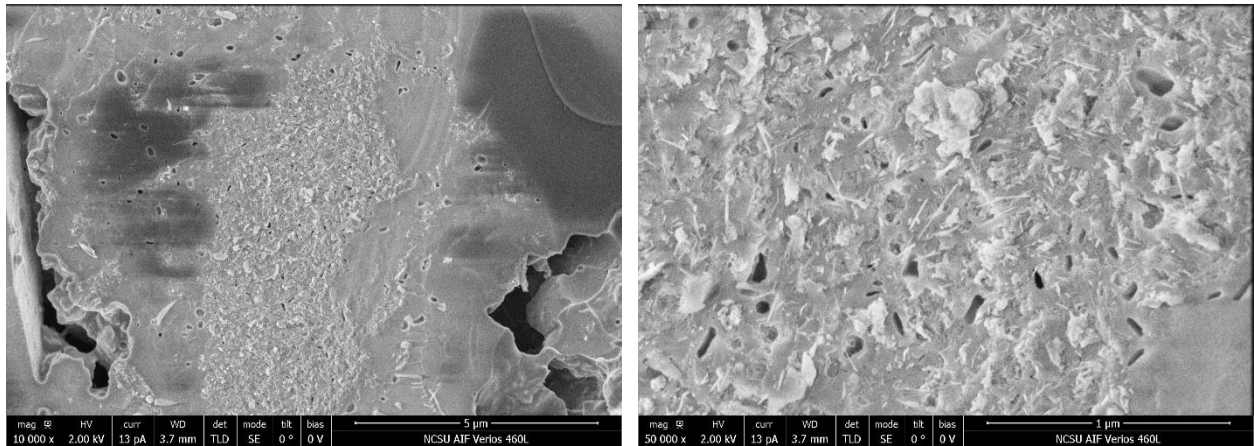


Figure 49. SEM cross section view of ceramic 1 wt% sample

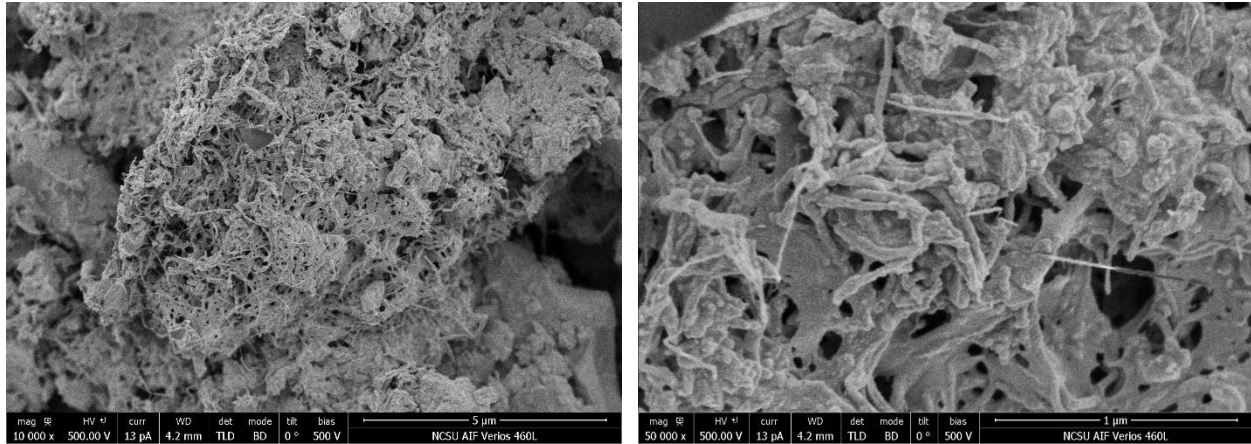


Figure 50. SEM cross section view of ceramic 5 wt% sample

The mechanical properties of these ceramic samples were tested with Knoop Hardness. Vickers Hardness would have been preferred but only Knoop was available at the time. All the samples were indented with a load of 100 gf. The optical microscope with imaging software was unavailable and the indentations had to be measured by eye using the x40 magnification lens on the hardness machine. Unfortunately, only the indentations from the 0 and 1 wt% sample were easy to locate with the magnification lens. The indentation for the other composites were barely visible and the ends of the diagonal were difficult to identify. Due to the possibility of human error during this measurement, these results are only considered preliminary and further testing is required before they can be confirmed. The preliminary hardness results can be seen in Table 10. The 1 wt% sample was much tougher than the control, but it also had a high standard deviation. However, even if we subtract the standard deviation from the average, we get a hardness of 6.45 GPa which is 438% higher than the pristine ceramic. While these results may not be completely accurate, they do suggest this method could possibly lead to major mechanical improvements with the composites. Further testing is required to confirm this claim.

Table 10. Preliminary Knoop Hardness Results

Samples	Knoop Hardness	Hardness (GPa)	Density (g/cm³)
0 wt%	149.7 ± 13.1	1.47 ± 0.13	1.22
1 wt%	1028 ± 372	10.1 ± 3.65	1.56

6.4 Summary

This was the final method used to successfully create BNNT-SiCN composites (up to 20 wt% BNNT). Ethanol was used to mix the preceramic powder and BNNT solution. The mixed solution was placed in the sonication bath for 5 minutes and then allowed to dry. This allowed us to avoid the aggressive nature of ball-milling, which was used to mix the nanotubes from the method used in Chapter 3. The 1 wt% ethanol mixed powder showed better BNNT dispersion from both natural and SEM inspections when compared to the 1 wt% ball-milling mixed powder. The composites were more dense and less porous than the pristine ceramic. However, the 1 wt% sample had the highest density at 1.56 g/cm³ which was 27.9% more dense than the control sample. The SEM images of the 1 wt% sample had a very dense and flat microstructure. It is not entirely clear why the 1 wt% was the densest of the composites. More samples need to be made to investigate the densification of the composites. A preliminary microhardness test was performed on the samples but only the 0 and 1 wt% samples could be measured. While this test may not be completely accurate, it did suggest the ethanol mixing method could lead to major mechanical improvements in the composites. Further testing is required to test this theory.

Chapter 7: Conclusion

7.1 Review of Manufacturing Methods

This thesis explored 4 unique manufacturing methods for developing boron nitride nanotube (BNNT) reinforced polymer-derived ceramic (PDC) composites. For each method, different aspects were investigated such as BNNTs effects on the composite's dimensions (density, shrinkage, mass loss), effectiveness of BNNT dispersion, and micro-hardness properties. The ultimate goal with this research is to develop a multi-functional ceramic composite that can endure the harsh environment of space. Such a material could be integrated into current space technologies and be implemented for a successful mission to Mars.

The *ball-milling mixing method* involved curing and ball-milling the precursor to create preceramic powder. The preceramic powder and BNNTs were then mixed using the ball-milling machine. This powder mixture was pressed and pyrolyzed to create the composites. A few significant findings with this method:

- High BNNT weight percentages (up to 25 wt%) composites were achievable with this technique. The weight percent of the composites was also easily controllable.
- The composites became denser (and less porous) as the BNNT weight percentage increased. The 25 wt% sample was 31% more dense and 30% less porous than the pristine ceramic. This densification was illustrated and confirmed with SEM images.
- The composites had a higher mechanical hardness than the ceramic sample. The 15 wt% sample had the highest recorded hardness at 3.49 GPa which was 200% harder than the pristine sample.
- It was difficult to locate the BNNTs in the composites under SEM. Which implies the ball-milling mixing was not effective at dispersing the BNNT in the preceramic powder. SEM

images also showed bent nanotubes which suggests ball-milling could be harmful to the BNNTs.

The *polymer infiltration and pyrolysis (PIP) method* required the BNNT to be dispersed in a liquid solution. The solution was filtered and a thin BNNT mat was created. This mat was infiltrated with the liquid precursor and then pyrolyzed to create the composites. Some discoveries from this method:

- Composites with very high BNNT weight percentages of about 35 wt% were attainable. But it is quite difficult to control the weight percentages with this manufacturing route.
- The composites increased density by 218% and decrease porosity by 30.2% when compared to the very porous BNNT mat. The cross-section SEM images shows the precursor was able to reach the center of the mat and fill up most of the empty space between the nanotubes. This implies the infiltration was mostly effective and a second cycle of infiltration should be used to fill up the remaining space.
- Unfortunately, the composites were not harder than the pristine ceramic material. The non-reinforced ceramic film was 347% harder than the composites. However, if viewed from a different perspective, the composites were harder than the BNNT mat. The composite had a hardness of 3.74 GPa which was 2330% higher than the hardness of the BNNT mat (which possibly contained epoxy during the hardness test).
- I believe this method can be revisited in the future once better quality BNNT mats have been made. High purity and aligned BNNT mats could help increase the composite's mechanical properties.

The *precursor mixing method* took advantage of the liquid phase of the polymer precursor. BNNT was added to the liquid precursor and mixed using a magnetic stir plate. It took about 4 days to fully disperse the BNNTs and no surfactant was needed. The mixed solution was cured in molds and then pyrolyzed to make the composites. A few observations with this method:

- Only composites with small weight percentages of BNNT (0.1 and 0.5 wt%) were possible. Adding too much BNNT in the precursor would make the solution too viscous and not allow the BNNT to fully disperse. Perhaps a compatible surfactant can be used in the future to help increase BNNT weight percentages.
- The composites formed more bubbles during the curing phase than the pristine polymer. In the future, vacuum should be applied when curing to reduce porosity. Also, the BNNTs began to separate from the precursor during the curing process, which means the dispersion can only be maintained if mixing is applied.
- The SEM images showed both the ceramic and composite samples having a fully dense ceramic matrix with a few micro-racks present. The BNNTs were only located in certain locations of the ceramic matrix. Some of the BNNTs were still entangled and cluster together, which means the BNNT dispersion was only somewhat effective.
- The 0.5 wt% composite had a hardness value 5.8% higher than the pristine ceramic. This slight increase in hardness was expected because only a small amount of BNNT was added to the composite. Higher weight percentages need to be tested to see if the hardness improvements scale linearly.

The *ethanol mixing method* returned to mixing the BNNTs with preceramic powder but with a different mixing technique. Ethanol was used to disperse both the powder and BNNT solution. This solution was placed in the sonication bath for 5 minutes to ensure good dispersion.

Once the ethanol evaporated, the mixed powder was collected, pressed and pyrolyzed to create the composites. With this method:

- Composites with high weight percentages of BNNT were achievable (up to 20 wt%). This is similar to the ball-milling mixing method, which had a 25 wt% sample.
- The density of the composites did not increase as the BNNT weight percent increased. Surprisingly, the 1 wt% sample had the highest density at 1.56 g/cm^3 which was 27.9% more dense than the control sample. Perhaps not enough pressure was used when powder pressing, or maybe the powder particles were not small enough. More samples should be made to revisit these results.
- The 1 wt% ethanol mixed powder was compared to the 1 wt% ball-milling mixed powder. The ethanol powder had a beige color while the ball-milling powder was white with tiny spots of dark grey clusters of BNNT. This implies the ethanol method is more effective at dispersing the BNNTs. These results were reinforced with SEM images of both mixed powders.
- Preliminary microhardness results suggest the 1 wt% composite was over 400% harder than the pristine ceramic. Which implies the BNNTs were able to significantly reinforce the ceramic matrix with this method. However, these were only initial results and more samples need to be tested before this claim can be made.

7.2 Future Work

Moving forward, I would recommend using the ethanol mixing method to make BNNT reinforced polymer derived ceramic composites. While this method is currently not optimized, it showed very promising results: high BNNT weight percentage composites were achievable, excellent BNNT dispersion within the powder, and potentially significant mechanical

improvements to the composites. For future samples, I would recommend ball-milling the cured precursor for a longer time (to create finer powder) and applying more pressure during the powder press to help reduce porosity.

The neutron radiation shielding capabilities of these BNNT ceramic composites can be tested next. North Carolina State University has a nuclear research reactor, known as the PULSTAR reactor, on main campus. This reactor has multiple beam ports with different neutron intensities. Multiple layers of the samples can be placed in front of the neutron beam to determine the effective thickness required to shield against neutron radiation. These results could be used to predict how effective the BNNT composites are at shielding against secondary neutrons in space, thus completing the final goal for this research.

References

- [1] Thibeault, Sheila A., et al. "Nanomaterials for radiation shielding." *Mrs Bulletin* 40.10 (2015): 836-841.
- [2] Pisacane, Vincent L. *The space environment and its effects on space systems*. American Institute of aeronautics and Astronautics, 2008.
- [3] "NASA's Mars Exploration Program." NASA, 3 June 2014, mars.nasa.gov.
- [4] Motion, Re-entry. "Returning from Space: Re-entry." (2016): 309-339.
- [5] Chancellor, Jeffery C., Graham BI Scott, and Jeffrey P. Sutton. "Space radiation: the number one risk to astronaut health beyond low earth orbit." *Life* 4.3 (2014): 491-510.
- [6] Bernardo, Enrico, et al. "Advanced ceramics from preceramic polymers modified at the nano-scale: a review." *Materials* 7.3 (2014): 1927-1956.
- [7] Bernard, Samuel, et al. "Kinetic modeling of the polymer-derived ceramics route: investigation of the thermal decomposition kinetics of poly [B-(methylamino) borazine] precursors into boron nitride." *The Journal of Physical Chemistry B* 110.18 (2006): 9048-9060.
- [8] Colombo, Paolo, et al. "Polymer-derived ceramics: 40 years of research and innovation in advanced ceramics." *Journal of the American Ceramic Society* 93.7 (2010): 1805-1837.
- [9] Wen, Qingbo, Zhaoju Yu, and Ralf Riedel. "The fate and role of in situ formed carbon in polymer-derived ceramics." *Progress in Materials Science* 109 (2020): 100623.
- [10] Wang, Xifan, et al. "Additive manufacturing of ceramics from preceramic polymers: A versatile stereolithographic approach assisted by thiol-ene click chemistry." *Additive manufacturing* 27 (2019): 80-90.

- [11] Seyferth, Dietmar, and Herbert Plenio. "Borasilazane polymeric precursors for borosilicon nitride." *Journal of the American Ceramic Society* 73.7 (1990): 2131-2133.
- [12] Su, Kai, et al. "Synthesis, characterization, and ceramic conversion reactions of borazine-modified hydridopolysilazanes: new polymeric precursors to silicon nitride carbide boride (SiNCB) ceramic composites." *Chemistry of materials* 5.4 (1993): 547-556.
- [13] Colombo P, editor. *Polymer derived ceramics: from nano-structure to applications*. DEStech Publications, Inc; 2010.
- [14] Riedel, Ralf, et al. "Silicon-based polymer-derived ceramics: synthesis properties and applications-a review dedicated to Prof. Dr. Fritz Aldinger on the occasion of his 65th birthday." *Journal of the Ceramic Society of Japan (日本セラミックス協会学術論文誌)* 114.1330 (2006): 425-444.
- [15] Ribeiro, M. J., et al. "Production of Al-rich sludge-containing ceramic bodies by different shaping techniques." *Journal of Materials Processing Technology* 148.1 (2004): 139-146.
- [16] Zhu, Yunzhou, et al. "Manufacturing 2D carbon-fiber-reinforced SiC matrix composites by slurry infiltration and PIP process." *Ceramics International* 34.5 (2008): 1201-1205.
- [17] Ichikawa, Hiroshi, Haruo Teranishi, and Toshikatsu Ishikawa. "Effect of curing conditions on mechanical properties of SiC fibre (Nicalon)." *Journal of materials science letters* 6.4 (1987): 420-422.
- [18] Bernard, Samuel. "Design, Processing and Properties of Ceramic Materials from Pre-ceramic Precursors, Nova Science Pub Inc." (2012).
- [19] Bill, Joachim, and Fritz Aldinger. "Precursor-derived covalent ceramics." *Advanced Materials* 7.9 (1995): 775-787.

- [20] Laine, Richard M., and Florence Babonneau. "Preceramic polymer routes to silicon carbide." *Chemistry of materials* 5.3 (1993): 260-279.
- [21] Harshe, Rahul, Corneliu Balan, and Ralf Riedel. "Amorphous Si (Al) OC ceramic from polysiloxanes: bulk ceramic processing, crystallization behavior and applications." *Journal of the European Ceramic Society* 24.12 (2004): 3471-3482.
- [22] Janakiraman, Narayanan, and Fritz Aldinger. "Fabrication and characterization of fully dense Si–C–N ceramics from a poly (ureamethylvinyl) silazane precursor." *Journal of the European Ceramic Society* 29.1 (2009): 163-173.
- [23] Shah, Sandeep R., and Rishi Raj. "Mechanical properties of a fully dense polymer derived ceramic made by a novel pressure casting process." *Acta Materialia* 50.16 (2002): 4093-4103.
- [24] ü nter Motz, G., Stephan Schmidt, and Steffen Beyer. "The PIP-process: precursor properties and applications." *Ceramic matrix composites* (2008).
- [25] Salvetti, Marie Gabrielle, et al. "Pyrolysis of a polysilazane precursor to SiCN ceramics." *Solid state ionics* 63 (1993): 332-339.
- [26] Blum, Yigal D., Kenneth B. Schwartz, and Richard M. Laine. "Preceramic polymer pyrolysis." *Journal of materials science* 24.5 (1989): 1707-1718.
- [27] Barroso, Gilvan, et al. "Polymeric and ceramic silicon-based coatings—a review." *Journal of materials chemistry A* 7.5 (2019): 1936-1963.
- [28] Schwartz, K. B., and David J. Rowcliffe. "Modeling density contributions in preceramic polymer/ceramic powder systems." *Journal of the American Ceramic Society* 69.5 (1986): C-106.

- [29] Greil, P., and M. Seibold. "Modelling of dimensional changes during polymer-ceramic conversion for bulk component fabrication." *Journal of materials science* 27.4 (1992): 1053-1060.
- [30] Barroso, Gilvan. *Thermal barrier coating by polymer-derived ceramic technique for application in exhaust systems*. Vol. 12. Cuvillier Verlag, 2018.
- [31] G. S. Barroso, W. Krenkel and G. Motz, Low thermal conductivity coating system for application up to 1000°C by simple PDC processing with active and passive fillers, *J. Eur. Ceram. Soc.*, 2015, 35, 3339
- [32] P. Greil and M. Seibold, Active-filler-controlled pyrolysis (AFCOP), in *Ceramic Transactions, Vol. 19, Advanced composite materials*, ed. M. D. Sacks, American Ceramic Society, Westerville, OH, 1991.
- [33] P. Greil, Near net shape manufacturing of polymer derived ceramics, *J. Eur. Ceram. Soc.*, 1998, 18, 1905.
- [34] Hennige, V. D., et al. "Shrinkage-free ZrSiO₄-ceramics: characterisation and applications." *Journal of the European Ceramic Society* 19.16 (1999): 2901-2908.
- [35] M. Lenz Leite, G. Barroso, M. Parchovianský, D. Galusek, E. Ionescu, W. Krenkel and G. Motz, Synthesis and characterization of yttrium and ytterbium silicates from their oxides and an oligosilazane by the PDC route for coating applications to protect Si₃N₄ in hot gas environments, *J. Eur. Ceram. Soc.*, 2017, 37, 5177.
- [36] Greil, Peter. "Active-filler-controlled pyrolysis of preceramic polymers." *Journal of the American Ceramic Society* 78.4 (1995): 835-848.
- [37] Torrey, Jessica D., et al. "Composite polymer derived ceramic system for oxidizing environments." *Journal of materials science* 41.14 (2006): 4617-4622.

- [38] Günthner, Martin, et al. "High performance environmental barrier coatings, Part I: Passive filler loaded SiCN system for steel." *Journal of the European Ceramic Society* 31.15 (2011): 3003-3010.
- [39] Schütz, Adelheid, et al. "High temperature (salt melt) corrosion tests with ceramic-coated steel." *Materials Chemistry and Physics* 159 (2015): 10-18.
- [40] Ohl, Christiane, et al. "Novel open-cellular glass foams for optical applications." *Journal of the American Ceramic Society* 94.2 (2011): 436-441.
- [41] Suda, H., et al. "Preparation and gas permeation properties of silicon carbide-based inorganic membranes for hydrogen separation." *Desalination* 193.1-3 (2006): 252-255.
- [42] Li, Zhongyan, Katsuki Kusakabe, and Shigeharu Morooka. "Pore structure and permeance of amorphous Si-CO membranes with high durability at elevated temperature." *Separation science and technology* 32.7 (1997): 1233-1254.
- [43] Konegger, Thomas, et al. "Asymmetric polysilazane-derived ceramic structures with multiscalar porosity for membrane applications." *Microporous and Mesoporous Materials* 232 (2016): 196-204.
- [44] Riedel, Ralf, et al. "Synthesis of dense silicon-based ceramics at low temperatures." *Nature* 355.6362 (1992): 714-717.
- [45] Soraru, G. D., et al. "Fabrication and Characterization of β -SiAlON Components from Polymeric Precursors." *MRS Online Proceedings Library Archive* 287 (1992).
- [46] Sorarù, Gian Domenico, Elisabetta Dallapiccola, and Gennaro D'Andrea. "Mechanical Characterization of Sol-Gel-Derived Silicon Oxycarbide Glasses." *Journal of the American Ceramic Society* 79.8 (1996): 2074-2080.

- [47] Renlund, Gary M., Svante Prochazka, and Robert H. Doremus. "Silicon oxycarbide glasses: Part II. Structure and properties." *Journal of Materials Research* 6.12 (1991): 2723-2734.
- [48] Clinton, D. J., and R. Morrell. "Hardness testing of ceramic materials." *Materials chemistry and physics* 17.5 (1987): 461-473.
- [49] Gong, Jianghong, Junqiu Wang, and Zhenduo Guan. "A comparison between Knoop and Vickers hardness of silicon nitride ceramics." *Materials Letters* 56.6 (2002): 941-944.
- [50] Güder, H. S., et al. "Vickers and Knoop Indentation Microhardness Study of β -SiAlON Ceramic." *Acta Physica Polonica, A*. 120.6 (2011).
- [51] Kim, Keun Su, et al. "Scalable manufacturing of boron nitride nanotubes and their assemblies: a review." *Semiconductor Science and Technology* 32.1 (2016): 013003.
- [52] Iijima, Sumio. "Helical microtubules of graphitic carbon." *nature* 354.6348 (1991): 56-58.
- [53] Rao, Chintamani Nagesa Ramachandra, et al. "Nanotubes." *ChemPhysChem* 2.2 (2001): 78-105.
- [54] Rubio, Angel, Jennifer L. Corkill, and Marvin L. Cohen. "Theory of graphitic boron nitride nanotubes." *Physical Review B* 49.7 (1994): 5081.
- [55] Chopra, Nasreen G., et al. "Boron nitride nanotubes." *Science* 269.5226 (1995): 966-967.
- [56] Golberg, Dmitri, et al. "Boron nitride nanotubes." *Advanced Materials* 19.18 (2007): 2413-2432.
- [57] Yamakov, Vesselin, et al. "Piezoelectric molecular dynamics model for boron nitride nanotubes." *Computational materials science* 95 (2014): 362-370.
- [58] Smith, Michael W., et al. "Very long single- and few-walled boron nitride nanotubes via the pressurized vapor/condenser method." *Nanotechnology* 20.50 (2009): 505604.

- [59] Smith, Michael W., Kevin Jordan, and Cheol Park. "Boron nitride nanotubes." (2012).
- [60] Nautiyal, Pranjali, et al. "High-temperature mechanics of boron nitride nanotube "Buckypaper" for engineering advanced structural materials." *ACS Applied Nano Materials* 2.7 (2019): 4402-4416.
- [61] Chapartegui, M., et al. "Analysis of the conditions to manufacture a MWCNT buckypaper/benzoxazine nanocomposite." *Composites Science and Technology* 72.4 (2012): 489-497.
- [62] Zhang, Jianwei, and Dazhi Jiang. "Influence of geometries of multi-walled carbon nanotubes on the pore structures of Buckypaper." *Composites Part A: Applied Science and Manufacturing* 43.3 (2012): 469-474.
- [63] McWilliams, Ashleigh D. Smith, et al. "Surfactant-assisted individualization and dispersion of boron nitride nanotubes." *Nanoscale Advances* 1.3 (2019): 1096-1103.
- [64] Singleterry, R. C. "Radiation engineering analysis of shielding materials to assess their ability to protect astronauts in deep space from energetic particle radiation." *Acta Astronautica* 91 (2013): 49-54.
- [65] Harrison, Courtney, et al. "Polyethylene/boron nitride composites for space radiation shielding." *Journal of applied polymer science* 109.4 (2008): 2529-2538.
- [66] Chawla, Krishan K. *Ceramic matrix composites*. Springer Science & Business Media, 2013.
- [67] Evans, A. G., and F. W. Zok. "The physics and mechanics of fibre-reinforced brittle matrix composites." *Journal of Materials science* 29.15 (1994): 3857-3896.
- [68] Berger, Marie, and Anthony Bunsell, eds. *Fine Ceramic Fibers*. CRC Press, 1999.

- [69] DiCarlo, James A. "Fibers for structurally reliable metal and ceramic composites." *JOM* 37.6 (1985): 44-49.
- [70] Chawla, Krishan K. "Reinforcements." *Composite Materials*. Springer, New York, NY, 1998. 6-71.
- [71] Crivelli-Visconti, I., and G. A. Cooper. "Mechanical properties of a new carbon fibre material." *Nature* 221.5182 (1969): 754-755.
- [72] Marshall, David B., and Anthony G. Evans. "Failure mechanisms in ceramic-fiber/ceramic-matrix composites." *Journal of the American Ceramic Society* 68.5 (1985): 225-231.
- [73] Brennan, John J., and Karl M. Prewo. "Silicon carbide fibre reinforced glass-ceramic matrix composites exhibiting high strength and toughness." *Journal of Materials Science* 17.8 (1982): 2371-2383.
- [74] Beyerle, Douglas S., et al. "Damage and failure in unidirectional ceramic-matrix composites." *Journal of the American Ceramic Society* 75.10 (1992): 2719-2725.
- [75] Evans, A. G., and F. W. Zok. "The physics and mechanics of fibre-reinforced brittle matrix composites." *Journal of Materials science* 29.15 (1994): 3857-3896.
- [76] Ramirez, Arthur P. "Carbon nanotubes for science and technology." *Bell Labs Technical Journal* 10.3 (2005): 171-185.
- [77] Xia, Z., et al. "Direct observation of toughening mechanisms in carbon nanotube ceramic matrix composites." *Acta Materialia* 52.4 (2004): 931-944.
- [78] Jakubinek, Michael B., et al. "Nanoreinforced epoxy and adhesive joints incorporating boron nitride nanotubes." *International Journal of Adhesion and Adhesives* 84 (2018): 194-201.

- [79] Yan, Haiyan, et al. "Enhanced thermal–mechanical properties of polymer composites with hybrid boron nitride nanofillers." *Applied Physics A* 114.2 (2014): 331-337.
- [80] Zhi, C. Y., et al. "Mechanical and thermal properties of polymethyl methacrylate-BN nanotube composites." *Journal of Nanomaterials* 2008 (2008).
- [81] Zhi, C. Y., et al. "Chemically activated boron nitride nanotubes." *Chemistry–An Asian Journal* 4.10 (2009): 1536-1540.
- [82] Zhi, C. Y., et al. "Boron nitride nanotubes: functionalization and composites." *Journal of Materials Chemistry* 18.33 (2008): 3900-3908.
- [83] Lin, Shuqiong, et al. "Covalent derivatization of boron nitride nanotubes with peroxides and their application in polycarbonate composites." *New Journal of Chemistry* 41.15 (2017): 7571-7577.
- [84] Bhuiyan, Md Mahedi Hasan, et al. "Boron nitride nanotube reinforced titanium metal matrix composites with excellent high-temperature performance." *Journal of Materials Research* 32.19 (2017): 3744.
- [85] Xue, Liang A., and I-Wei Chen. "Superplastic Alumina at Temperatures below 1300° C Using Charge-Compensating Dopants." *Journal of the American Ceramic Society* 79.1 (1996): 233-238.
- [86] Huang, Qing, et al. "Enhancing superplasticity of engineering ceramics by introducing BN nanotubes." *Nanotechnology* 18.48 (2007): 485706.
- [87] Bansal, Narottam P., Janet B. Hurst, and Sung R. Choi. "Boron nitride nanotubes-reinforced glass composites." *Journal of the American Ceramic Society* 89.1 (2006): 388-390.

- [88] Jia, Yujun, et al. "Thermal properties of polymer-derived ceramic reinforced with boron nitride nanotubes." *Journal of the American Ceramic Society* 102.12 (2019): 7584-7593.
- [89] Zhi, Chunyi, et al. "Specific heat capacity and density of multi-walled boron nitride nanotubes by chemical vapor deposition." *Solid state communications* 151.2 (2011): 183-186.
- [90] Yang, Jinshan, et al. "Strong and ultra-flexible polymer-derived silicon carbonitride nanocomposites by aligned carbon nanotubes." *Ceramics International* 42.12 (2016): 13359-13367.
- [91] Duke, Philip, et al. "Study of the physical properties of type IV gypsum, resin-containing, and epoxy die materials." *The Journal of prosthetic dentistry* 83.4 (2000): 466-473.